Zhang *et al.*
Cell Communication and Signaling (2024) 22:416
https://doi.org/10.1186/s12964-024-01797-2

Cell Communication and Signaling

RESEARCH

Open Access

Involvement of HDAC2-mediated *kcnq2/kcnq3* genes transcription repression activated by EREG/EGFR-ERK-Runx1 signaling in bone cancer pain

Zi-Xian Zhang[1†], Yue Tian[1,2†], Song Li[1], Hong-Bo Jing[1], Jie Cai[1,2], Min Li[3*] and Guo-Gang Xing[1,2*]

Abstract

Bone cancer pain (BCP) represents a prevalent symptom among cancer patients with bone metastases, yet its underlying mechanisms remain elusive. This study investigated the transcriptional regulation mechanism of Kv7(KCNQ)/M potassium channels in DRG neurons and its involvement in the development of BCP in rats. We show that HDAC2-mediated transcriptional repression of *kcnq2/kcnq3* genes, which encode Kv7(KCNQ)/M potassium channels in dorsal root ganglion (DRG), contributes to the sensitization of DRG neurons and the pathogenesis of BCP in rats. Also, HDAC2 requires the formation of a corepressor complex with MeCP2 and Sin3A to execute transcriptional regulation of *kcnq2/kcnq3* genes. Moreover, EREG is identified as an upstream signal molecule for HDAC2-mediated *kcnq2/kcnq3* genes transcription repression. Activation of EREG/EGFR-ERK-Runx1 signaling, followed by the induction of HDAC2-mediated transcriptional repression of *kcnq2/kcnq3* genes in DRG neurons, leads to neuronal hyperexcitability and pain hypersensitivity in tumor-bearing rats. Consequently, the activation of EREG/EGFR-ERK-Runx1 signaling, along with the subsequent transcriptional repression of *kcnq2/kcnq3* genes by HDAC2 in DRG neurons, underlies the sensitization of DRG neurons and the pathogenesis of BCP in rats. These findings uncover a potentially targetable mechanism contributing to bone metastasis-associated pain in cancer patients.

Keywords Bone cancer pain, Kv7(KCNQ)/M potassium channels, Transcriptional repression, Histone deacetylase 2, Methyl CpG binding protein 2, Epiregulin, Epidermal growth factor receptor, Dorsal root ganglia

Introduction

Bone cancer pain (BCP) resulting from primary bone tumors or bone metastases is one of the most severe and intractable types of chronic pain. Understanding the mechanisms that cause it can inform drug development that may improve quality of life of patients. We previously have found that suppression of Kv7(KCNQ)/M potassium channels in dorsal root ganglion (DRG) neurons contributes to the hyperexcitability of DRG neurons and the pathogenesis of BCP in rats [1, 2]. However, the molecular mechanism underlying the transcriptional regulation of Kv7(KCNQ)/M channels in DRG neurons and its role in BCP remain unknown.

†Zi-Xian Zhang and Yue Tian contributed equally to this work.

*Correspondence:
Min Li
liminanesth@bjmu.edu.cn
Guo-Gang Xing
ggxing@bjmu.edu.cn
[1] Department of Neurobiology, School of Basic Medical Sciences, Peking University Health Science Center and Neuroscience Research Institute, Peking University, Beijing, China
[2] Key Laboratory for Neuroscience, Ministry of Education of China & National Health Commission of China, Beijing 100191, China
[3] Department of Anesthesiology, Peking University Third Hospital, Beijing 100191, China

The Kv7(KCNQ)/M channels are a family of voltage-gated potassium channels consisting of five family members (Kv7.1-Kv7.5) encoded by *kcnq*1-5 genes, among them the KCNQ2 and KCNQ3 are expressed exclusively in the nervous system [3], and co-assembled KCNQ2 and KCNQ3 subunits constitutes the native M channel in most neurons [4]. This channel generates a species of low-threshold, slowly activating, slowly deactivating, and non-inactivating K^+ current (M-current), which acts as a "brake" to regulate the action potential (AP) firing and the neuronal excitability [5]. Suppression of M-current increases the neuronal excitability, whereas their enhancement has a silencing effect [6, 7].

Histone acetylation modifications, a common form of epigenetic modification, mainly occur on conserved lysine residues at the H3 and H4 N-terminal tail, which are catalyzed by histone acetyltransferases (HATs) and histone deacetylases (HDACs) [8]. Histone acetylation alters the condensed chromatin into a more relaxed structure, and promotes gene transcription, whereas histone deacetylation tightly condenses chromatin resulting in gene silencing [9]. HDAC2, a member of class I HDACs has been implicated in various pain models including bone cancer pain [10, 11]. The catalytic activity of HDACs is mostly dependent on its association with multiprotein complexes such as switch-insensitive 3a (Sin3A) [12, 13]. The methyl-CpG binding protein 2 (MeCP2) recruits transcriptional corepressors including Sin3A/HDAC2 to the promoter region of a targeted gene resulting in gene silencing [14, 15]. These findings raise the possibility that HDAC2, which needs to form corepressor complex with MeCP2 and Sin3A, plays a vital role in *kcnq2* and *kcnq3* genes transcriptional repression.

Epiregulin (EREG) that signals through the epidermal growth factor receptor (EGFR) is involved in pain processing [16]. The downstream effects of EGFR are mediated by a number of signaling pathways including ERK cascade [17], which regulates multiple pain responses. The activation of ERK signaling is implicated in the phosphorylated modification of Runx1 [18, 19], a Runt domain transcription factor that is required for the differentiation of nociceptors and the pathogenesis of persistent pain [20, 21]. Runx1 has been shown to transcriptionally regulate HDAC2 expression in breast cancer tissues [22]. We hence hypothesized a strong link between the activation of EREG/EGFR-ERK-Runx1 signaling and the HDAC2-mediated transcriptional repression of *kcnq2* and *kcnq3* genes in DRG neurons.

We here investigated the transcriptional regulation mechanism of Kv7(KCNQ)/M potassium channels in DRG neurons and its involvement in BCP in rats. We uncovered that the HDAC2-mediated transcriptional repression of *kcnq2* and *kcnq3* genes, induced by the activation of EREG/EGFR-ERK-Runx1 signaling, contributes to the sensitization of DRG neurons and the pathogenesis of BCP in rats.

Materials and methods

Animals

Adult male and female Sprague–Dawley rats weighing 180 to 220 g at the beginning of the experiments were provided by the Department of Experimental Animal Sciences, Peking University Health Science Center. All rats were housed in separated cages, and the room was kept at 24° ± 1 °C and 50 to 60% humidity under a 12-h light/12-h dark cycle with ad libitum access to food and water. All experiments were approved by the Animal Care and Use Committee of Peking University (Approval number: BCJB0019) and performed in accordance with both the National Institutes of Health Guide for the Care and Use of Laboratory Animals and the ARRIVE (Animal Research: Reporting of In Vivo Experiments) guidelines.

Animal model of bone cancer pain

A rat model of bone cancer pain was established by intratibial injection of syngeneic MRMT-1 rat mammary gland tumor cells as previously described [21, 23]. Briefly, after being anesthetized with 1% pentobarbital sodium [50 mg/kg, intraperitoneal (i.p.)], the left tibia of rat was carefully exposed and a 23-gauge needle was inserted in the canal of the bone. It was then removed and replaced with a long, thin blunt needle attached to 10-μl Hamilton syringe containing the medium to be injected. A volume of 5 μl MRMT-1 rat mammary gland tumor cells (1×10^7) or vehicle (PBS) was injected into the tibial bone cavity. After injection, the site was sealed with bone wax, and the wound was finally closed. Any rats exhibiting motor deficiency or lack of pain hypersensitivity after tumor cell inoculation, as well as those that died during the experiments, were excluded from the study.

Intrathecal catheterization

Intrathecal catheterization is a reliable approach for the delivery of drugs or vectors into the DRG of rats [24, 25], and chronic lumbar catheterization of the spinal subarachnoid space in rodents offers several advantages for intrathecal delivery of drugs upon repeated administration [26–28]. Consequently, intrathecal catheterization is well suited for long-term behavioral and pharmacological studies. Under general anesthesia via intraperitoneal injection (i.p.) of pentobarbital sodium (50 mg/kg), implantation of an intrathecal catheter was performed as described in previous studies [21, 23]. Briefly, a PE-10 polyethylene catheter was implanted between the L5 and L6 vertebrae to reach the lumbar enlargement of the spinal cord. The outer part of the catheter was plugged

and fixed onto the skin upon closure of the wound. All surgical procedures were performed under sterile conditions. Rats showing neurological deficits after the catheter implantation were euthanized. After recovery for 3 to 7 days, drugs or vectors were intrathecally injected via the implanted catheter in a 10-μl volume of solution (for lentivirus injection, 20 μl) followed by 10 μl of vehicle for flushing. Each injection lasted for at least 5 min. After an injection, the needle remained in situ for 2 min before being withdrawn.

Drug administration and lentivirus infection

Trichostatin A (50 μg/kg), sodium butyrate (10 mM, 30 mM, 100 mM, 300 mM), or an equal dose of vehicle was intrathecally administered to the BCP model rats on day 7 after tumor cells inoculation, once per day for seven consecutive days. Recombinant lentivirus expressing either HDAC2 shRNA linked with GFP (LV-shHDAC2), MeCP2 shRNA linked with ZsGreen (LV-shMeCP2), or EGFR shRNA linked with ZsGreen (LV-shEGFR) was respectively constructed by Obio Technology (Shanghai, China, for LV-shHDAC2) and Likeli Technology (Beijing, China, for LV-shMeCP2 and LV-shEGFR), using pLVX-mCMV-GFP vector or pLVX-mCMV-ZsGreen vector as indicated. Lentivirus, including LV-shHDAC2 (LV-GFP as control), LV-shMeCP2 (LV-ZsGreen as control), LV-shEGFR (LV-ZsGreen as control), or the control virus was intrathecally administered to the BCP model rats at a final titer of 5×10^8 transducing units/mL (in a 20-μl volume of solution), on day 7 after tumor cells inoculation. Sin3A siRNA (2.5 μg), Runx1 siRNA (2.5 μg), or an equal dose of scramble siRNA in a 10-μl mixture with in vivo jetPEI transfection reagent (Polyplus-transfection SA, Illkirch, France) was intrathecally administered to the BCP model rats on day 7 after tumor cells inoculation, twice per day for seven consecutive days. EREG (50 μg/ml × 10 μl), or an equal dose of vehicle was intrathecally administrated to naïve rats, once per day for four consecutive days. In some experiments, LV-shEGFR (or the control LV-ZsGreen) was intrathecally administered to the EREG-treated rats, at a final titer of 5×10^8 transducing units/mL (in a 20-μl volume of solution), on day 7 before intrathecal EREG application. In another experiment, Runx1 siRNA (2.5 μg, in a 10-μl volume solution) was intrathecally administered to the EREG-treated rats on day 1 before intrathecal EREG application, twice per day for five consecutive days. AG1478 (50 μM × 10 μl), or an equal dose of vehicle was delivered intrathecally to BCP model rats on day 10 after tumor cells inoculation, once per day for four consecutive days. SCH772984 (15 mM × 10 μl), or an equal dose of vehicle was intrathecally administered to BCP model rats on day 7 after tumor cells inoculation, twice per day for seven consecutive days. In some experiments, SCH772984 (15 mM × 10 μl) was intrathecally administered to the EREG-treated rats on day 1 before intrathecal EREG application, twice per day for five consecutive days. See Supplementary Tables S1 and S2 for chemicals and sequences of the shRNA.

Behavioral tests

All behavioral experiments were performed in a blinded fashion (the tester was blinded to treatment groups). Animals were randomly placed into treatment groups with 8 to 15 rats per treatment per trial in consideration of the excluded ones, and the number for statistical analysis did not include the excluded rats.

Mechanical hypersensitivity, as a behavioral sign of bone cancer pain, was assessed by measuring 50% paw withdrawal threshold (PWT) as described in previous reports [21, 29]. The 50% PWT in response to a series of von Frey filament (Stoelting, Wood Dale, IL) was determined by the up-and-down method [30]. Eight von Frey filaments with about equal logarithmic incremental (0.224) bending forces were chosen (0.41 g, 0.70 g, 1.20 g, 2.00 g, 3.63 g, 5.50 g, 8.50 g, and 15.10 g). The 50% PWT was calculated using the following formula: 50% PWT (g) $=10^{[X,+\kappa\delta]}$, where X_f is the value of the final von Frey filament used (in log units), κ is a value measured from the pattern of positive/negative response, and $\delta=0.224$, which is the average interval (in log units) between the von Frey filaments. If an animal did not respond to highest von Frey filament, then the value was recorded as 15.10 g. In rats, the mechanical hypersensitivity is assessed by measuring the 50% PWT in responseto von Frey filaments stimuli, and an allodynic rat is defined as that whose 50% PWT is less than 4.0 g (i.e., withdrawal in response to non-noxious tactile stimulus).

Thermal hyperalgesia of the hind-paws was tested as described by Hargreaves [31]. In brief, rats were allowed to acclimate for a minimum of 30 min before testing. A radiant heat source was focused onto the plantar surface the hind paw. Measurements of paw withdrawal latency (PWL) were taken by a timer that was started by the activation of the heat source and stopped when withdrawal of the paw was detected with a photodetector. A maximal cutoff time of 30 s was used to prevent unnecessary tissue damage. Three measurements of PWL were taken for each hind paw and were averaged as the result of each test session. The hind paw was tested alternately with > 5-min intervals between consecutive tests.

Locomotor function was assessed with the inclined-plate test, according to the method reported by Rivlin and Tator [32]. Briefly, animals were placed crosswise to the long axis of an inclined plate. The initial angle of the inclined plate was 50°. The angle was then adjusted in 5°

increments. The maximum angle of the plate on which the rat maintained its body position for 5 s without falling was determined. In this study, the inclined plate test was performed for all behavioral experiments in which the animals received intrathecal drugs.

Primary culture and acute dissociation of DRG neurons

Primary cultures of DRG neurons were performed according to a method described previously [23]. Briefly, rats (2 weeks old) were euthanized and DRG tissues were dissected from the lumbar spinal segments. The ganglia were digested with collagenase type IA (3 mg/mL, Sigma-Aldrich) for 50 min and 0.25% trypsin (type II-S, Sigma-Aldrich) for another 10 min at 37℃. After terminating the enzymatic treatment by Dulbecco's modified Eagle's medium (DMEM) plus 10% fetal bovine serum, ganglia were dissociated with a polished Pasteur pipette, and the suspension of ganglia was sieved through a filter to remove debris and centrifuged at 800 rpm for 3 min. The resuspended cells were plated on 35-mm dishes coated with poly-D-lysine (0.5 mg/mL; Sigma-Aldrich), kept for 3 h, and replaced with neurobasal growth medium containing B27 supplement, 0.5 mM L-glutamax (Sigma-Aldrich), penicillin (100 U/mL), and streptomycin (100 mg/mL). The cells were kept at 37 ℃ in an incubator with 5% CO_2 and 95% air for 3 days before further treatment. Cultures were fed daily with neurobasal growth medium containing B27 supplement.

Acute dissociation of DRG neurons was performed as described in our previous reports [21, 23]. Briefly, neurons were isolated from the L4 and L5 DRG tissues of adult rats and were digested using the same procedure as described for primary cell culture above. The dissociated cells were used for patch-clamp recording within 3 to 8 h of plating.

RNA sequencing and analysis

Total RNA was extracted from ipsilateral lumbar (L4-L5) DRG tissues collected from both BCP model rats ($n=6$) and the control PBS-treated rats ($n=6$) on day 14 post-surgery, where DRG tissues from 2 animals were pooled during dissection. RNA sequencing (RNA-seq) was performed by Beijing Genomics Institute (BGI). Briefly, DRG tissues were dissociated and TRIzol reagent was utilized to extract total RNA following the manufacturer's instructions. Total RNA was isolated using the RNeasy mini kit (Qiagen, Germany), and the RNA-seq library preparation from 1 μg of total RNA was performed with TruSeq RNA Sample Preparation Kit (Illumina, America) according to the protocol provided by the manufacturer. In briefly, the poly A-containing mRNA molecules were purified and fragmented into small pieces using divalent cations at 94 °C for 8 min. Then, library quantity was assessed using a Qubit 2.0 Fluorometer (Invitrogen, United States) and validated using an Agilent 2100 bioanalyzer (Agilent Technologies, America) to confirm the insert size and to calculate the mole concentration. The standardized gene expression measurement known as TPM (Transcript per kilobase per million mapped reads) was performed to identify differentially expressed genes (DEGs) among the groups. When comparing DEGs between two groups, the fold change (FC) of TPM values was first calculated and then took the base two logarithmic [log2(FC)]. We selected genes with $\log2(FC) \geq 1.0$ as the threshold for significant differences in gene expression, as referenced as a difference of at least two-fold between the two groups. Accurate transcript results were obtained by assembly. The expression of each gene or transcript was determined. Finally, relevant pathways were identified through Kyoto Encyclopedia of Genes and Genomes (KEGG) enrichment analysis and gene ontology (GO) analysis. KEGG pathway analysis was performed to analyze the advanced functions of differentially expressed genes (DEGs), and GO enrichment analysis labels gene with a function, such as molecular function, biological process, or cellular component, and also, KEGG analysis provides annotation information of signal transduction and disease pathways for genes, thus providing a basis for gene function and pathway research.

RNA extraction and RT-qPCR

Total RNA was extracted from the rat L4/L5 DRG tissues with TRIzol reagent (Invitrogen). Reverse transcription was performed with oligo deoxythymidine (oligo-dT) primers and Moloney murine leukemia virus (M-MLV) reverse transcriptase (Promega) according to the manufacturer's protocol. Polymerase chain reaction (PCR) primer sequences are listed in Supplementary Table S3. Real-time quantitative PCR (RT-qPCR) was performed with GoTaq qPCR Master Mix (Promega) and an ABI 7500 Fast Real-Time PCR Detection System (Applied Biosystems). Briefly, a 20-μl PCR reaction that included 1 μl of complementary DNA, 10 μl of GoTaq qPCR Master Mix, and 0.5 μl of each primer was used and adjusted to the final volume with RNase-free water. β-actin in parallel for each run was used as an internal control. The reactions were set up on the basis of the manufacturer's protocol. PCR conditions were incubation at 95℃ for 2 min followed by 40 cycles of thermal cycling (10 s at 95℃, 20 s at 58℃, and 10 s at 72℃). The relative expression ratio of mRNA was quantified via the $2^{-\Delta\Delta CT}$ method.

Chromatin immunoprecipitation (ChIP)

ChIP assays were performed using the Magna ChIP Assay kit (Millipore) in accordance with the manufacturer's

protocol [33, 34]. In brief, the homogenized solution from L4/L5 DRG tissues was treated with 1% formaldehyde at room temperature for 30 min to cross-link DNA and associated proteins, and terminated by the addition of 125 mM glycine. After two washes with ice-cold PBS containing protease inhibitors, the tissues were pelleted by centrifugation and resuspended in 1×sodium dodecyl sulfate (SDS) lysis buffer containing 1% SDS, 10 mM EDTA, 50 mM Tris–HCl (pH 8.1), 10 ml/ml protease inhibitors cocktail, and 10 ml/ml phosphatase inhibitors. After incubation for 15 min at 4 °C, the lysates were sonicated (10 s each for 6 times) to shear chromatin to DNA fragments between 250–1000 bp as assessed by agarose gel electrophoresis. After centrifugation, the chromatin samples (the supernatant) were diluted tenfold in ChIP dilution buffer containing 1% Triton X-100, 2 mM/l EDTA, 150 mM l NaCl, 20 mM l Tris–HCl (pH 8.1), 10 ml/ml protease inhibitor cocktail and 10 ml/ml phosphatase inhibitor (Thermo Scientific, Madison, WI), and an aliquot was saved as the input DNA. Then, the samples were incubated with protein G agarose at 4 °C overnight, and were subjected to immunoprecipitation with the corresponding antibody (10 μg for each antibody), including rabbit anti-HDAC2 antibody (Abcam, MA), rabbit anti-MeCP2 antibody (Abcam, MA), rabbit anti-acH3 antibody (Merck Millipore, Germany), rabbit anti-acH4 antibody (Merck Millipore, Germany), and rabbit anti-Runx1 antibody (Abcam, MA), at 4℃ overnight. Samples were washed three times in lysis buffer (50 mM Tris, pH 7.4, 1 M NaCl, 1 mM EDTA, 0.1% SDS, 1% NP-40, and 0.5% sodium deoxycholate), and the beads were then resuspended in lysis buffer and treated with proteinase K at 45 °C for 45 min. Coprecipitated DNAs were purified using a TIANquick Maxi Purification Kit (TIANGEN Biotech, China) and eluted in 50 μl nuclease-free water. Ten percent of the sample was used for immunoprecipitation as the input, while normal rat IgG was used as the negative control. The immunoprecipitated DNA (protein-DNA complex) was eluted, purified, and quantified by RT-qPCR, and all values were normalized to the input. The binding sites of HDAC2 in the promoter region of both *kcnq2* and *kcnq3* genes were predicted from the PROMO (http://alggen.lsi.upc.es) and JASPAR databases (http://jaspar2016.genereg.net). Fold enrichment was assessed using RT-qPCR and the $2^{-\Delta\Delta CT}$ method. The primers used are listed in Supplementary Table S3.

DNA agarose gel electrophoresis

1×of Tris–acetate-EDTA buffer (TAE, Thermo Fisher Scientific, USA) diluted with ddH_2O was used as a buffer system, 1% agarose gels in TAE buffer containing 5 μl of 10,000×GelRed (Beyotime Biotechnology, China) was used and poured into the electrophoresis tank, allow the gels to dry, pull out the comb, and 5 μl of the samples was mixed with 1 μl of 6×DNA loading buffer (Takara, China) and transferred to wells. The Trans2K Plus II DNA Marker (TransGen Biotechnology, China) was also transferred to the sides of wells. The gels were run for 30 min at 100 V and were placed on the EC3 gel imaging system (UVP, USA) and set up with 365 nm UV to detect the electrophoretic bands, and the results were observed and photographed.

Enzyme-linked immunosorbent assay

To collect tissues for EREG content analysis, the animals were rapidly decapitated, and the L4/L5 DRG tissues was excised and placed into a Petri dish containing dry-ice-cold homogenizing buffer. Then they were homogenized in cold extraction Tris-buffered saline (pH 8.0) containing 1% NP-40, 10% glycerol, 0.5 mM sodium metavanadate, 1 mM phenylmethylsulfonyl fiuoride, 10 mg/mL aprotinin, and 1 mg/mL leupeptin. The lysates were centrifuged for 15 min at 12000 g, and a commercially available enzyme-linked immunosorbent assay (ELISA) kit (NOVUS, USA) was used to detect EREG content in the supernatants. This monoclonal antibody shows no cross-reactivity with other neurotrophins (NT-3, NT-4, brain-derived neurotrophic factor or nerve growth factor). EREG content in the DRG tissues was normalized to the amount of total protein, which was determined at the same time as the ELISA using a BCA protein assay kit (Pierce, Rockford, IL). Because the solid DRG tissues were obtained and only the weight but not volume could be measured, therefore the EREG level was expressed in pg/mg total protein rather than pg/mL volume.

Western blot

Cultured DRG neurons or the dissected rat L4/5 DRG tissues were immediately homogenized in ice-cold lysis buffer containing 50 mM tris (pH 8.0), 150 mM NaCl, 1% NP-40 (Sigma-Aldrich), 0.5% sodium deoxycholate (Sigma-Aldrich), 0.1% SDS, 1% protease inhibitor cocktail and 1% protein phosphatase inhibitor cocktails (Thermo Scientific, Madison, WI). After being rotated at 4℃ for 1 h, the homogenates were centrifuged at 12,000 rpm for 10 min to yield the total protein extract in the supernatant, and the supernatant was analyzed. The sample containing 60 μg of protein was denatured and then separated through SDS-PAGE using 10% to 12% separating gels and transferred to a polyvinylidene fluoride (PVDF) membrane (Sigma-Aldrich). The membranes were blocked with 5% nonfat milk in TBST [20 mM tris–HCl (pH 7.5), 150 mM NaCl, and 0.05% Tween 20] for 60 min at room temperature, and then incubated with the following primary antibodies at 4℃ overnight:

rabbit anti-KCNQ2 antibody(1:1000, Abcam), rabbit anti-KCNQ3 antibody (1:1000, Abcam), rabbit anti-HDAC1 antibody (1:1000, Abcam), rabbit anti-HDAC2 antibody (1:1000, Merck Millipore), rabbit anti-HDAC3 antibody (1:1000, Abcam), rabbit anti-MeCP2 antibody (1:500, Abcam), rabbit anti-phospho-ERK1/2 antibody (1:1000, Cell Signaling Technology), rabbit anti-ERK1/2 antibody (1:2000, Cell Signaling Technology), rabbit anti-phospho-Runx1 (Ser249) (1:1000, Cell Signaling Technology), rabbit anti-Runx1(1:2000, Abcam), rabbit anti-EGFR antibody (1:1000, Abcam), mouse anti-β-actin (1:3000, Santa Cruz Biotechnology). The blots were washed in TBST and then were incubated in horseradish peroxidase-conjugated secondary antibody (goat anti-rabbit/mouse or rabbit anti-goat IgG, 1:2000, ZSGB-BIO). Protein bands were visualized using an enhanced chemiluminescence detection kit (Pierce) followed by autoradiography using Hyperfilm MP (Santa Cruz Biotechnology). The band was quantified with a computer-assisted imaging analysis system (ImageJ, NIH).

Immunofluorescence staining

To prepare DRG tissues for immunofluorescence analysis, deeply anesthetized rats were intracardially perfused with 50 ml of 0.1 M phosphate buffer (PB) followed by 500 ml of cold 4% paraformaldehyde (in 0.1 MPB, pH 7.4). After perfusion, the ipsilateral L4/5 DRG tissues were removed quickly, post-fixed for 4 h in the perfusion fixative and cryoprotected in 30% sucrose (in 0.1 M PBS) overnight at 4 °C. Serial frozen DRG Sects. (10 μm thick) were cut on a cryostat and thaw-mounted on gelatin-coated slides for immunostaining processing. To prepare cultured DRG neurons, the cells were rinsed for 5 min with PBS and fixed for 10 min with 4% paraformaldehyde in PBS at room temperature.

For immunostaining, the tissues or cultured cells were washed three times in PBS for 5 min each and blocked in 10% goat serum (in 0.1 M PBS) with 0.3% Triton-X 100 for 1 h at room temperature. Then, tissues or cultured cells were incubated with the corresponding primary antibody (see Supplementary Table S1) in PBS at 4 °C overnight, which includes rabbit anti-KCNQ2 (1:200, Abcam), rabbit anti-KCNQ3 (1:200, Abcam), rabbit anti-mouse NeuN (1:200, Sigma-Aldrich), mouse anti-pig GFAP (1:200, Cell Signaling Technology), mouse anti-NF200 (1:200, Sigma-Aldrich), mouse anti-CGRP (1:200, Abcam), rabbit anti-HDAC2 (1:200, Abcam), rabbit anti-MeCP2 (1:200, Abcam), goat anti-EGFR antibody (1:200, GeneTex), rabbit anti-Runx1(1:200, Abcam), goat anti-Sin3A (1:200, R&D systems). For IB4 immunostaining, after three washes in PBS, the tissues were incubated with FITC-conjugated Bandeiraea simplicifolia IB4 (10 μg/ml) for 3 h. Then, after 3 washes in PBS, tissues or cultured cells were incubated with the following appropriate secondary antibody at room temperature for 1 h: Alexa Fluor 647 donkey anti-goat (1:500, Jackson ImmunoResearch), Alexa 647 donkey anti-mouse IgG (1:200, Jackson ImmunoResearch), Alexa Fluor 488 donkey anti-mouse (1:500, Jackson ImmunoResearch), Cy3 donkey anti-rabbit (1:500, Jackson ImmunoResearch), Cy3 donkey anti-goat IgG (1:200, Jackson ImmunoResearch), TRITC goat anti-rabbit IgG (1:200, ZSGB-BIO), FITC goat anti-mouse IgG (1:200, ZSGB-BIO), FITC donkey anti-goat IgG (1:200, Jackson ImmunoResearch). In some experiments, the tissues or cultured cells were counterstained with the nuclear marker DAPI (100 ng/mL) carrying blue fluorescence for 10 min at room temperature. The tissues were mounted in Gel/Mount medium. Visualization of fluorescence signal was performed by confocal microscopy at excitation wavelengths of 488 nm (green), 543 nm (red) as well as 405 nm and 647 nm (blue). At least four fields per well/section were analyzed to establish reproducibility.

Whole-cell patch clamp recordings

Whole-cell patch clamp recordings from acutely dissociated or primary cultured DRG neurons were performed at room temperature using an EPC-10 amplifier and Patch-Master software (HEKA, Freiburg, Germany). Patch pipettes were pulled from borosilicate glass capillaries with a tip resistance of 5 to 8 MΩ when filled with internal solution containing (in mM) 80 K-acetate, 30 KCl, 1 $CaCl_2$, 3 $MgCl_2$, 3 EGTA, 3 Mg-ATP, and 40 HEPES (4-(2-Hydroxyethyl) piperazine-1-ethanesulfonic acid), adjusted to pH 7.4 with KOH. The external solution contained (in mM) 144 NaCl, 2.5 KCl, 2 $CaCl_2$, 0.5 $MgCl_2$, 5 HEPES, and 10 glucose, adjusted to pH 7.4 with NaOH. Membrane currents and voltage were measured with pipette and membrane capacitance cancellation, filtered at 2 kHz, and digitized at 10 kHz. Resting membrane potential (RMP) was measured immediately after rupture of the cell membrane in whole-cell patch mode.

Under voltage-clamp recording, cells were clamped at -70 mV, and series resistance was compensated 70% ~ 90%. The membrane capacitance was read from the amplifier by Patch-Master software (HEKA) for determining the size of cells and calculating the current density. Following the protocol described in our previous study [2], M-currents in DRG neurons were studied by holding the membrane potential at -20 mV and applying a 1-s hyperpolarizing pulse from -20 mV to -110 mV in increments of -10 mV at 4 s-intervals. The M-current was defined as the outward current sensitive to 3 μM XE-991, and the amplitude of M-currents was measured from deactivation current records at -50 mV as the difference between the average of a 10-ms segment, taken

10 to 20 ms into the hyperpolarizing step, and the average during the last 10 ms of that step. Mean instantaneous and steady-state I-V relationships for M-current were obtained by measuring the current at the beginning and end of the voltage pulse, respectively. Deactivation of M-current was best-fitted by 2 exponentials, with 2-time constants, τ_{fast} and τ_{slow}. Concentration response curves for XE-991 were constructed by plotting percentage inhibition of M-current as a function of drug concentration plotted on a log scale. Smooth curves were fitted to these data with the Hill equation of the form $y = y_{max}\, x^n/(\kappa^n + x^n)$, where x is the concentration, y is the percentage inhibition, and y_{max} is the maximal value of y (at saturation); in the fitting procedure y_{max} was constrained not to exceed 100%. The term κ is the IC_{50} (the concentration giving half-maximal inhibition) and n (Hill slope) is the power term related to the slope of the curve.

Under current-clamp recording, the cells were held at 0 pA, and the firing threshold (rheobase) of DRG neurons was first measured by a series of 100-ms depolarizing current injection in 5-pA steps from 0 pA to elicit the first action potential (AP), and then, a large depolarizing current pulse (1-s, 2-fold rheobase) was delivered to elicit the cell generating sufficient firing. To further examine the neuron firing properties, a series of 500-ms depolarizing current pulses were delivered to the cell, in 50-pA steps from 0 to 400 pA, to elicit ascending AP firing, and the firing rate (spikes/second) was calculated in each injected depolarizing current pulse. In this study, we measured RMP, rheobase (the current threshold for eliciting the first AP), threshold potential (TP), inter-spike intervalss (ISI), AP amplitude, afterhyperpolarization (AHP) amplitude, AHP duration at 80% repolarization ($AHP_{80\%}$ duration), and frequency of AP to evaluate the intrinsic electrophysiological properties of DRG neurons. Origin software 9.0 (OriginLab Corporation, Northampton, MA) was used for data analysis and fitting.

Statistical analysis

Statistical analyses were performed with GraphPad Prism 9.0 for Windows (GraphPad Software, La Jolla, CA). All quantitative biochemical data and immunofluorescence staining are representative of at least three independent biological replicates. Shapiro–Wilk tests were used to assess normality in the distribution (Gaussian distribution) for each group, and only the data were normally distributed and variances were similar between groups to be compared were subjected to parametric statistical tests. Two-tailed unpaired Student's *t* test was used for the comparison of the mean values between two groups. One-way analysis of variance (ANOVA) with Dunnett's *post hoc* test or Tukey's *post hoc* test; or two-way ANOVA with Sidak's *post hoc* test or Tukey's *post hoc* test, as indicated in the text was used for multiple comparison. All data are reported as means ± SEM, and differences with $p < 0.05$ were considered statistically significant. $^{*}p < 0.05$, $^{**}p < 0.01$, $^{***}p < 0.001$; ns, not significant. All statistical data are presented in Supplementary Table S4, and all source data are presented in Supplementary Table S5.

Results

Identification of HDAC2-mediated transcriptional repression of Kv7(KCNQ)/M potassium channels in DRG neurons and its role in bone cancer-induced pain in rats

Previously, we have reported that the suppression of Kv7(KCNQ)/M potassium channels in DRG neurons contributed to the pathogenesis of bone cancer pain (BCP) in a rat model [2]. Although we have found a decreased abundance of both KCNQ2 and KCNQ3 protein in ipsilateral lumber 4 and lumber 5 (L4/5) DRG tissues, as well as a reduction of M-current density in L4/5 DRG neurons of BCP model rats (Fig. S1A-D), however the intrinsic functional characteristics of channels inferred by voltage-dependence and kinetics of M-currents, and by the concentration dependence of XE-991-inhibition of M-currents, are not altered in BCP model rats (Fig. S1E-J). Together with the decreased expression of KCNQ2 and KCNQ3 mRNA levels in ipsilateral L4/5 DRG tissues (Fig. S1K and L), we speculated that a transcriptional repression of Kv7(KCNQ)/M potassium channels may occur in the DRG neurons of BCP model rats.

In the present study, we aimed to investigate the transcriptional regulation mechanism of Kv7(KCNQ)/M channels in DRG neurons and its involvement in the pathogenesis of BCP in rats. First, we performed RNA-seq analysis on the DRG tissues of both BCP model rats and the control PBS-treated rats. Total RNA was extracted from ipsilateral L4/5 DRG tissues collected from both BCP model rats ($n = 6$) and PBS-treated rats ($n = 6$) on day 14 post-surgery, where the DRG tissues from 2 animals were pooled during dissection. The principal component analysis (PCA) of gene expression demonstrated that the two groups of samples were markedly separated (Fig. S2A). The differentially expressed genes (DEGs) in the DRG tissues were presented in the heat map (Fig. S2B), among them, there were a large number of interacting genes that were simultaneously regulated (Fig. S2C). A total of 166 DEGs were identified between the two groups, of which, 97 genes were up-regulated and 69 genes were down-regulated (Fig. S2D and E). Moreover, Kyoto Encyclopedia of Genes and Genomes (KEGG) enrichment analysis revealed that the DEGs were mainly enriched in the following pathways, including pathways in cancer, EGFR tyrosine kinase inhibitor resistance pathway, ErbB signaling pathway, Ras signaling pathway, and

MAPK signaling pathway, and also, all of these pathways were significantly upregulated in BCP model rats (Fig. 1A). Moreover, the results from gene ontology (GO) analysis revealed that the up-regulated genes were mainly involved in mitogen-activated protein kinase activity, transcriptional corepressor binding, nuclear localization sequence binding, histone deacetylase (HDAC) binding, etc. (Fig. 1B). It has been documented that HDACs can remove the acetyl residues from histones to compact the chromatin structure, and inhibit gene transcription

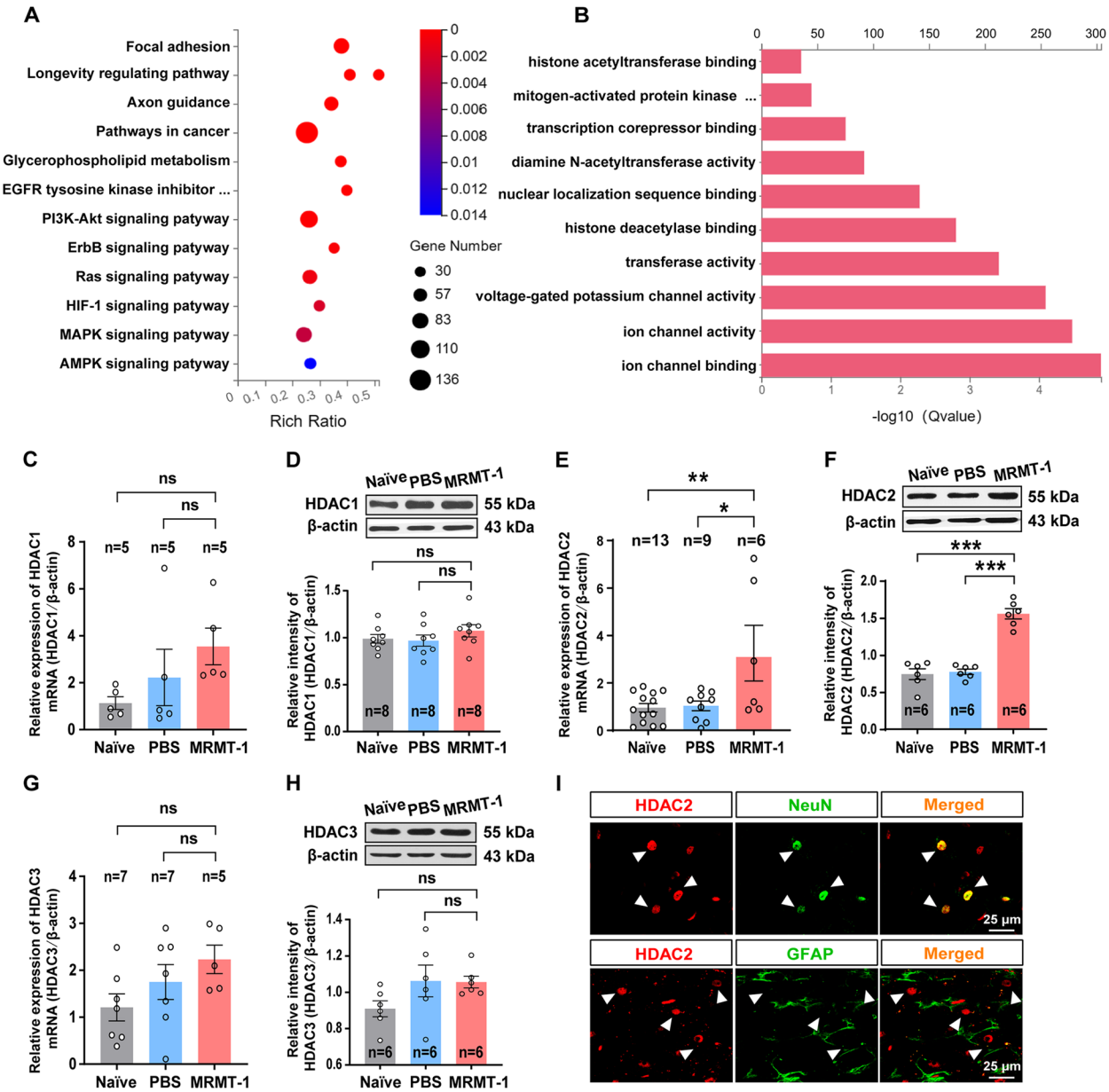

Fig. 1 Identification of the involvement of HDAC2 in bone cancer pain. (**A**) The enriched pathways of differentially expressed genes (DEGs) in the DRG tissues revealed by Kyoto Encyclopedia of Genes and Genomes (KEGG) enrichment analysis of RNA-sequencing (RNA-seq) data between the bone cancer pain (BCP) model rats and the control PBS-treated rats ($n = 6$ rats per group). (**B**) The molecular functions of the upregulated DEGs in the DRG tissues of BCP model rats predicted by gene ontology (GO) analysis of RNA-seq data ($n = 6$ rats per group). (**C**-**H**) RT-qPCR and Western blot analyses of the mRNA and protein abundance of HDAC1 (**C** and **D**), HDAC2 (**E** and **F**), and HDAC3 (**G** and **H**) in ipsilateral L4/5 DRG tissues obtained from naïve, PBS-, and MRMT-1-treated rats, performed at 14 days after surgery ($n = 5$–13 rats per group). Upper in (**D**, **F**, and **H**): Representative blots are shown. (**I**) Representative images show the immunofluorescence staining of HDAC2 with NeuN (upper) and GFAP (lower), respectively, in L4/5 DRG tissues of naïve rats ($n = 3$ rats per group). Scale bar = 25 mm. Data are presented as mean ± SEM. $^{*}p < 0.05$, $^{**}p < 0.01$, $^{***}p < 0.001$; ns, not significant, one-way ANOVA followed by Dunnett's *post hoc* test for (**C**)-(**H**). See also Fig. S1-S5

[35, 36]. Class I HDACs, in particular HDAC2 is found highly correlated to the pathology of persistent pain [37–41]. Thus, we performed DEGs' gene–gene interaction network analysis for *Hdac2*, and identified multiple potential interacting genes including *Mecp2*, *Sin3a*, *Mapk3*, *Runx1*, etc. (Fig. S2F). These genes, in turn, could interconnect with much more genes, including genes encoding potassium channel (*Kcnq, Kcnh, Kcnj, Kcnb*), epidermal growth factor (EGF) family ligands and receptors (*Ereg, Egfr*), acetyltransferase (*Hat1, Nat8f3*), and so on (Fig. S2G). These data raise the possibility that HDAC2 may be involved in the transcriptional regulation of Kv7(KCNQ)/M potassium channels in the DRG neurons of BCP model rats.

To test this hypothesis, we performed RT-qPCR and Western blotting assays for HDAC2 in ipsilateral L4/5 DRG tissues on day 14 post-surgery among naïve rats, PBS-treated rats, and MRMT-1-treated rats (BCP model rats). As expected, we indeed found a significant increase in both mRNA and protein abundance of HDAC2 but not HDAC1 and HDAC3 (the two other members of Class I HDACs that mainly expressed in the DRG neurons), in ipsilateral L4/5 DRG tissues of BCP model rats compared with controls (Fig. 1C-H). With respect to the cellular localization of HDAC2 in the DRG, immunofluorescent staining revealed that HDAC2 was colocalized with NeuN-positive neurons instead of GFAP-positive astrocytes in the DRG (Fig. 1I). In the DRG neurons, HDAC2 was predominantly localized in the cell nuclei, and was widely distributed among various types of DRG neurons, including $NF200^{+}$-, $CGRP^{+}$-, and $IB4^{+}$-cells (Fig. S3A-C). Also, a statistical increase in the mean fluorescence intensity of HDAC2 was observed in these three types of DRG neurons from BCP model rats relative to those from controls (Fig. S3D-F). These results demonstrate an increased expression of HDAC2 in the DRG neurons of BCP model rats, and provide basic evidence for the involvement of HDAC2-mediated transcriptional repression of *kcnq2* and *kcnq3* (*kcnq2/kcnq3*) genes in the pathogenesis of BCP.

Numerous studies have shown that HDACs mainly act on histones, lower the acetylation of histones, strengthen the binding of histones with DNA strands, and thus indirectly inhibit gene transcription. Here, two HDAC2-binding sites were identified in the *kcnq2* gene promoter (site 1: -1361 ~ -1206 bp of exons; site 2: -297 ~ -126 bp of exons), while one HDAC2-binding site were identified in the *kcnq3* gene promoter (-540 ~ -169 bp of exons), by using chromatin immunoprecipitation (ChIP) followed by DNA agarose gel electrophoresis (Fig. S3G). Also, the relative enrichment of HDAC2 in the *kcnq2* gene promoter was significantly increased at site 2 but not site 1 (Fig. S3H and I). Similarly, the relative enrichment of HDAC2 was prominently increased in the *kcnq3* gene promoter (Fig. S3J). Thus, the site 2 but not site 1 of the *kcnq2* gene promoter was examined in the following experiments. Consistent with the increased enrichment of HDAC2 in the *kcnq2/kcnq3* genes promoter, a significant reduction of both acetylated histone 3 (H3Kac) and acetylated histone 4 (H4Kac) was observed in the *kcnq2* and *kcnq3* genes promoter (Fig. S3K-N), indicating the histone deacetylation modification of *kcnq2/kcnq3* genes promoter was promoted by HDAC2 in the DRG neurons of BCP model rats.

To further determine the involvement of HDAC2-mediated histone deacetylation modification in *kcnq2/kcnq3* genes transcription repression and its roles in the pathogenesis of BCP in rats, we first examined the effects of trichostatin A (TSA), a pan-HDACs inhibitor, on KCNQ2/KCNQ3 expression, DRG neuronal excitability, and pain hypersensitivity in BCP model rats. TSA (50 μg/kg body weight) or vehicle was intrathecally administered to BCP model rats on day 7 after MRMT-1 tumor cells inoculation, once per day for seven consecutive days, and the following biochemical analyses and electrophysiological recordings were respectively performed on day 14 after tumor cells inoculation. The results showed that intrathecal TSA substantially reversed the reduction of KCNQ2 and KCNQ3 abundance in ipsilateral L4/5 DRG tissues of BCP model rats, at both mRNA and protein levels, compared to the controls (Fig. S4A-D). Meanwhile, intrathecal TSA also rescued the decreased M-current density (6.60 ± 0.41 pA/pF TSA *vs.* 3.01 ± 0.25 pA/pF vehicle, $P < 0.0001$) and the enhanced neuronal excitability of ipsilateral L4/5 DRG neurons, inferred from the decrease of action potential (AP) frequency, the increases of inter-spike intervals (ISI), AP amplitude, after hyperpolarization (AHP) amplitude, AHP duration at 80% repolarization ($AHP_{80\%}$ duration), the threshold potential (TP) and rheobase (Fig. S4E-I), and also, alleviated pain hypersensitivity, assessed by paw withdrawal threshold (PWT) in response to von Frey filaments stimuli (Fig. S4J, post-drug, 10.36 ± 0.73 g TSA *vs.* 4.20 ± 0.53 g vehicle, $P < 0.0001$) and paw withdrawal latency (PWL) in response to radiant heat stimulation (Fig. S4K, post-drug, 13.54 ± 0.82 s TSA *vs.* 8.67 ± 0.54 s vehicle, $P = 0.0055$), in BCP model rats that received intrathecal TSA compared to vehicle. Moreover, the results from inclined-plate test revealed that the animal's locomotor function was not impaired after intrathecal TSA application (Fig. S4L). Next, we explored the effects of intrathecal sodium butyrate (SB), a relative specific inhibitor of class I HDACs, on KCNQ2/KCNQ3 expression, DRG neuronal excitability, and pain hypersensitivity in BCP model rats. SB (at the dose of 10 mM, 30 mM, 100 mM, 300 mM) or vehicle was intrathecally administered to BCP model rats

on day 7 after MRMT-1 tumor cells inoculation, once per day for seven consecutive days, and the following biochemical analyses and electrophysiological recordings were respectively performed on day 14 after tumor cells inoculation. Likewise, intrathecal SB reversed the reduction of KCNQ2 and KCNQ3 abundance in ipsilateral L4/5 DRG tissues of BCP model rats, at both mRNA and protein levels, and also, rescued the decrease of M-current density and the increase of DRG neuronal excitability, and abrogated the pain hypersensitivity of MRMT-1 tumor-bearing rats, at the higher doses (100 mM and 300 mM) but not the lower doses (10 mM and 30 mM) (Fig. S5).

Furthermore, we investigated the effects of knockdown HDAC2 on KCNQ2/KCNQ3 expression, DRG neuronal excitability, and pain sensitivity in BCP model rats. Knockdown of HDAC2 in DRG neurons was performed by intrathecal administration of lentivirus expressing HDAC2 small hairpin RNA (shRNA) linked with GFP (LV-shHDAC2) to BCP model rats on day 7 after tumor cells inoculation, and the DRG tissues were collected on day 14 after tumor cells inoculation for further immunofluorescence staining, biochemical analyses or electrophysiological recordings. Using immunofluorescence staining, real-time quantitative PCR (RT-qPCR) and Western blotting analysis from either cultured rat DRG neurons at 48 h after transfected with LV-shHDAC2 (Fig. S6A-D), or the DRG tissues of BCP model rats on day 7 after received intrathecal LV-shHDAC2 (Fig. S6E-H), we saw a significant decrease of HDAC2 abundance at both mRNA and protein levels, validating the efficiency of knockdown HDAC2 in DRG neurons by LV-shHDAC2 application. Accompanied with the knockdown of HDAC2 by LV-shHDAC2, we observed a significant increase in the enrichment of both acetylated histone 3 (H3Kac) and acetylated histone 4 (H4Kac) in the *kcnq2* and *kcnq3* genes promoter, in BCP model rats that received intrathecal LV-shHDAC2 compared to the control LV-GFP (Fig. 2A-D), indicating that knockdown of HDAC2 inhibits the histone deacetylation modification of *kcnq2/kcnq3* genes promoter in the DRG neurons of BCP model rats. Also, we found a significant increase in the abundance of KCNQ2 and KCNQ3 expression, at both mRNA and protein levels, in ipsilateral L4/5 DRG tissues of BCP model rats that received intrathecal LV-shHDAC2 (Fig. 2E-H). Consistently, the M-current density was increased (5.08 ± 0.42 pA/pF LV-shHDAC2*vs*. 3.80 ± 0.18 pA/pF LV-GFP, $P = 0.0002$), whereas the neuronal excitability inferred from the following intrinsic electrogenic properties, including AP frequency, ISI, AP amplitude, AHP amplitude, $AHP_{80\%}$ duration, the threshold potential and rheobase, was reduced in ipsilateral L4/5 DRG neurons of BCP model rats that received intrathecal LV-shHDAC2 compared to the control LV-GFP (Fig. 2I-O). Moreover, the mechanical hypersensitivity assessed by the decreased PWT in response to von Frey filaments stimuli was alleviated in the BCP model rats treated with intrathecal LV-shHDAC2 (Fig. 2P), in spite of that the thermal hyperalgesia, as measured by the reduced PWL in response to radiant heat stimulation, was not relieved (Fig. 2Q). The results from inclined-plate test revealed that the animal's locomotor function was not impaired after intrathecal LV-shHDAC2 treatment (Fig. 2R). These results indicate that knockdown of HDAC2 by intrathecal LV-shHDAC2 effectively rescues the transcriptional repression of Kv7(KCNQ)/M

(See figure on next page.)

Fig. 2 Knockdown of HDAC2 in DRG neurons disrupts the transcriptional repression of *kcnq2* and *kcnq3* genes, reduces the neuronal excitability and attenuates pain hypersensitivity in bone cancer pain model rats. (**A**-**D**) ChIP-qPCR assays for the enrichment of acetylated histone 3 (H3Kac) and acetylated histone 4 (H4Kac) in the *kcnq2* and *kcnq3* genes promoter, in ipsilateral L4/5 DRG tissues obtained from bone cancer pain (BCP) model rats that received intrathecal LV-shHDAC2 or the control LV-GFP, performed at 14 days after tumor cells inoculation. (**A** and **B**) for H3Kac ($n = 4$–6 rats per group); (**C** and **D**) for H4Kac ($n = 8$ rats per group). (**E**–**H**) RT-qPCR and Western blot analyses of the mRNA and protein abundance of KCNQ2 and KCNQ3 in ipsilateral L4/5 DRG tissues obtained from BCP model rats that received intrathecal LV-shHDAC2 or the control LV-GFP, performed at 14 days after tumor cells inoculation. (**E** and **F**) for KCNQ2 ($n = 6$–9 rats per group); (**G** and **H**) for KCNQ3 ($n = 6$–7 rats per group). Upper in (**F** and **H**): Representative blots are shown. (**I**-**O**) Electrophysiological analyses of M-currents (**I** and **M**) and neuronal excitability (**J**-**O**) in ipsilateral L4/5 DRG neurons of BCP model rats that received intrathecal LV-shHDAC2 or the control LV-GFP, recorded at 14 days after tumor cells inoculation. (**I** and **J**) Representative traces of M-currents (**I**) and neuronal action potentials (**J**) evoked by a large depolarizing current pulse (1-s, 2-fold AP rheobase) are shown. Scale bar = 100 pA, 300 ms for (**I**), and 20 mV, 100 ms for (**J**). (**K** and **L**) Analysis of neuronal firing rate (spikes/second) elicited by a series of 500-ms depolarizing current pulses (in 50-pA steps from 0 to 400 pA). (**K**) Representative traces of evoked action potentials (APs) by 100 pA, 200 pA, and 300 pA depolarizing current pulses are shown. Scale bar = 20 mV, 200 ms. (**M**–**O**) Plots of M-current density, frequency of APs, inter-spike intervals (ISI), AP amplitude, after hyperpolarization (AHP) amplitude, AHP duration at 80% repolarization ($AHP_{80\%}$ duration) (**M**), threshold potential (**N**), and rheobase (**O**) ($n = 20$–30 cells from six rats per group). (**P** and **Q**) Assessment of ipsilateral PWT (**P**) and PWL (**Q**) of BCP model rats that received intrathecal LV-shHDAC2 or the control LV-GFP, performed at 14 days after tumor cells inoculation ($n = 11$ rats per group). (**R**) Assessment of animal's locomotor function before and after intrathecal lentivirus administration ($n = 11$ rats per group). Data are presented as mean ± SEM. $^{*}p < 0.05$, $^{**}p < 0.01$, $^{***}p < 0.001$, unpaired *t* test for (**A**)-(**H**) and (**M**)-(**O**); two-way ANOVA with Sidak's *post hoc* test for (**L**) and (**P**)-(**R**). See also Fig. S6

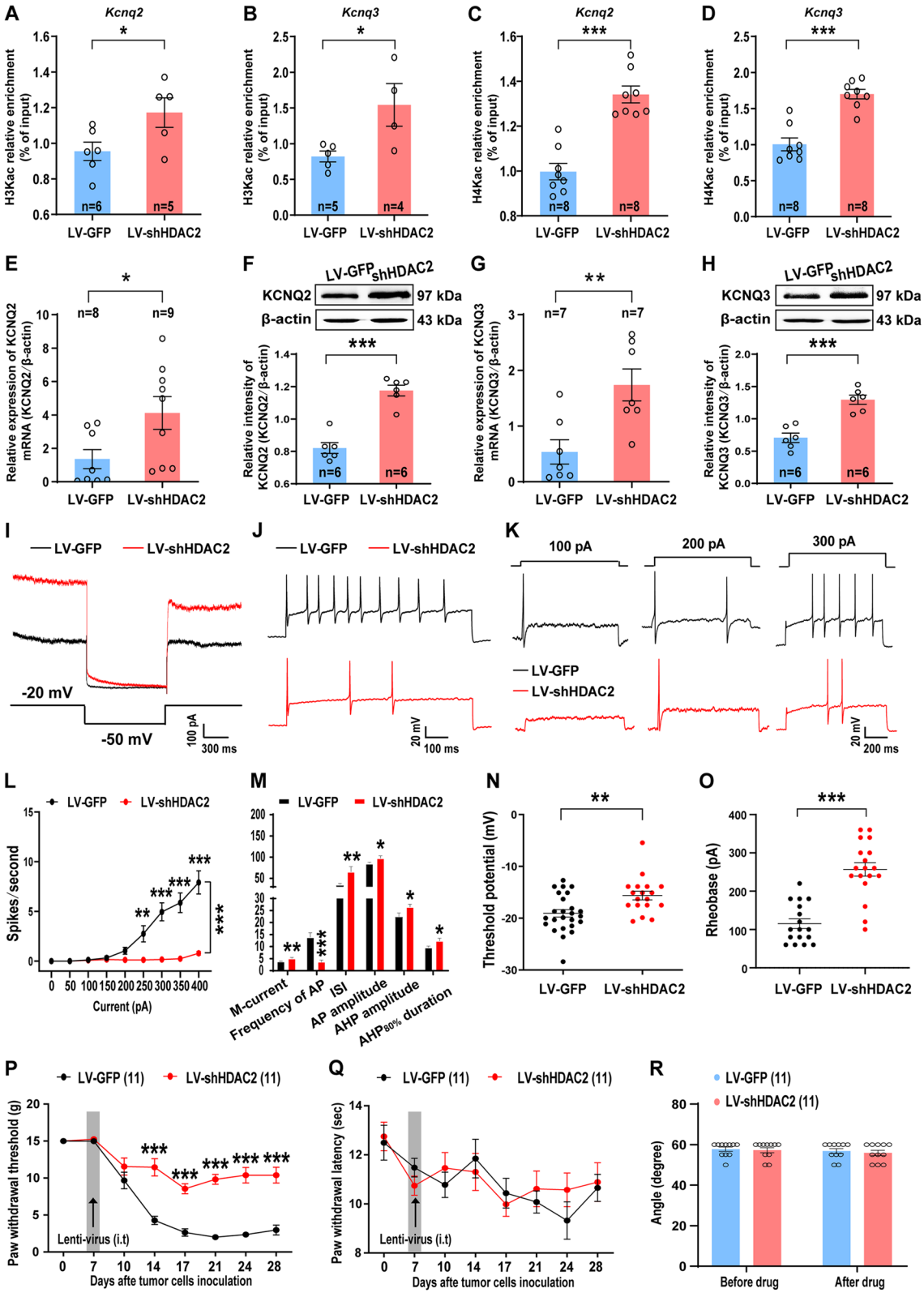

Fig. 2 (See legend on previous page.)

channels in DRG neurons of BCP model rats via inhibiting the histone deacetylation modification of *kcnq2/kcnq3* genes promoter, thereby reducing the neuronal hyperexcitability and pain hypersensitivity in tumor-bearing rats, supporting the contribution of HDAC2-mediated transcriptional repression of Kv7(KCNQ)/M channels in DRG neurons to the pathogenesis of BCP in rats.

Necessary of MeCP2 for HDAC2-mediated transcriptional repression of Kv7(KCNQ)/M potassium channels in DRG neurons and its role in bone cancer-induced pain in rats

Several lines of evidence have shown that HDACs cannot directly bind to the promoter region of the target gene, it needs to form complexes with other proteins to exert its transcriptional repression function [42]. The canonical HDAC2 complex is switch-insensitive 3a (Sin3A) [12, 13], and the methyl-CpG binding protein 2 (MeCP2) recruits transcriptional corepressors such as Sin3A/HDAC2 to the promoter region of a targeted gene, resulting in gene silencing [14, 15, 43]. In fact, as shown in aforementioned data of DEGs' gene–gene interaction network analysis for *hdac2*, *mecp2* and *sin3a* are predicted interacting genes with *hdac2* (Fig. S2F). To further determine the involvement of MeCP2 in HDAC2-mediated transcriptional repression of Kv7(KCNQ)/M potassium channels in DRG neurons and its contribution to bone cancer-induced pain in rats, we first examined the distribution of MeCP2 in DRG neurons and the alterations of MeCP2 abundance in the DRG of BCP model rats. Using immunofluorescent staining with MeCP2, HDAC2, KCNQ2/KCNQ3 and DAPI (4′,6-diamidino-2-phenylindole, the nuclear marker) from cultured rat DRG neurons, we observed an extensive co-localization of MeCP2 with HDAC2 and KCNQ2/KCNQ3 in the DRG neurons (Fig. S7A). Also, using ChIP-qPCR assay from ipsilateral L4/5 DRG tissues of naïve-, PBS-, and MRMT-1-treated rats, we found a significant increase in relative enrichment of MeCP2/HDAC2 corepressor complex in the *kcnq2* and *kcnq3* genes promoter, in MRMT-1 rats compared to the naïve and PBS controls (Fig. S7B and C), indicating an enhanced binding of MeCP2/HDAC2 corepressor complex to the *kcnq2* and *kcnq3* genes promoter of DRG neurons in BCP model rats. Moreover, the results of immunofluorescent staining showed that, MeCP2 was localized among various types of DRG neurons, including $NF200^{+}$-, $CGRP^{+}$-, and $IB4^{+}$-cells (Fig. S7D-F), and an increased mean fluorescence intensity of MeCP2 was observed among these three types of DRG neurons in BCP model rats compared to naïve and PBS controls (Fig. S7G-I). Likewise, an increased abundance of MeCP2 protein was found in ipsilateral L4/5 DRG tissues of MRMT-1 rats (Fig. S7J). Besides, an increased enrichment of MeCP2 in the *kcnq2* and *kcnq3* genes promoter was seen in ipsilateral L4/5 DRG neurons of MRMT-1 rats, as determined by ChIP-qPCR assay (Fig. S7K and L), implying an enhanced binding of MeCP2 to the promoter region of *kcnq2* and *kcnq3* genes.

Next, we investigated the effects of knockdown MeCP2 in DRG neurons on the HDAC2-mediated transcriptional repression of Kv7(KCNQ)/M channels, as well as, on the neuronal hyperexcitability and pain hypersensitivity in BCP model rats. Knockdown of MeCP2 in DRG neurons was performed by intrathecal administration of lentivirus expressing MeCP2 shRNA linked with ZsGreen (LV-shMeCP2) on day 7 after tumor cells inoculation, and the DRG tissues were collected on day 7 after intrathecal lentivirus application. Using immunofluorescence staining, RT-qPCR and Western blotting analysis from either cultured rat DRG neurons at 48 h after transfected with LV-shMeCP2 (Fig. S8A-D), or the DRG tissues of BCP model rats on day 7 after received intrathecal lentivirus application (Fig. S8E-H), we saw a significant decrease of MeCP2 abundance at both mRNA and protein levels, validating the efficiency of knockdown MeCP2 in DRG neurons by LV-shMeCP2 application. Along with the knockdown of MeCP2 in DRG neurons, a significant decrease in relative enrichment of MeCP2/HDAC2 corepressor complex in the *kcnq2* and *kcnq3* genes promoter was found in ipsilateral L4/5 DRG neurons in BCP model rats that received intrathecal LV-shMeCP2 compared to the control LV-ZsGreen (Fig. 3A and B), indicating a reduced binding of MeCP2/HDAC2 corepressor complex to the *kcnq2* and *kcnq3* genes promoter of DRG neurons in BCP model rats, as a result of knockdown MeCP2 in DRG neurons. Consistently, a remarkable increase in the enrichment of both H3Kac and H4Kac in the *kcnq2* and *kcnq3* genes promoter was seen in BCP model rats that received intrathecal LV-shMeCP2 (Fig. 3C-F), implying a decreased histone deacetylation modification occurred in the *kcnq2/kcnq3* genes promoter of DRG neurons in BCP model rats, resulted from the knockdown of MeCP2 in DRG neurons. Moreover, a prominent increase in the abundance of KCNQ2 and KCNQ3 expression, at both mRNA and protein levels, was found in ipsilateral L4/5 DRG tissues of BCP model rats that received intrathecal LV-shMeCP2 compared to the control LV-ZsGreen (Fig. 3G-J). As a result, the M-current density was increased (7.14 ± 0.42 pA/pF LV-shHDAC2 *vs.* 4.50 ± 0.27 pA/pF LV-GFP, $P < 0.0001$), whereas the neuronal excitability was reduced (inferred from the intrinsic electrogenic properties, including the decreased AP frequency as well as the increased ISI, AP amplitude, AHP amplitude, $AHP_{80\%}$ duration, the threshold potential and rheobase), in ipsilateral L4/5 DRG neurons of BCP model rats that received intrathecal LV-shMeCP2 relative to the

controls (Fig. 3K-Q). Expectedly, the mechanical hypersensitivity, assessed by the decreased PWT in response to von Frey filaments stimuli, was alleviated in the BCP model rats that received intrathecal LV-shMeCP2 application (Fig. 3R), in spite of that the thermal hyperalgesia, as measured by the reduced PWL in response to radiant heat stimulation, was not relieved (Fig. 3S). The results from inclined-plate test revealed that the animal's locomotor function was not impaired after intrathecal lentivirus treatment (Fig. 3T). These results indicate that knockdown of MeCP2 by intrathecal LV-shMeCP2 effectively restores the HDAC2-mediated transcriptional repression of Kv7(KCNQ)/M channels in DRG neurons of BCP model rats, subsequently reduces the neuronal hyperexcitability and pain hypersensitivity in tumor-bearing rats, evidencing the necessary of MeCP2 for the HDAC2-mediated transcriptional repression of Kv7(KCNQ)/M channels in DRG neurons and its role in bone cancer-induced pain in rats.

Involvement of MeCP2/Sin3A/HDAC2 corepressor complex in the transcriptional repression of Kv7(KCNQ)/M potassium channels in DRG neurons and in the pathogenesis of bone cancer-induced pain in rats

The catalytic activity of HDACs is mainly dependent on its incorporation into multiprotein co-repressor complexes, among them the Sin3A/HDAC corepressor is widely implicated to regulate synaptic plasticity [44]. The Sin3A/HDAC corepressor complex is a multiprotein complex comprised of several proteins like HDAC1, HDAC2, and MeCP2 [45]. The MeCP2 recruits transcriptional corepressors, such as Sin3A/HDAC2, to the promoter region of a targeted gene resulting in gene silencing [14, 15, 43]. The aforementioned data from DEGs' gene–gene interaction network analysis for *Hdac2* (Fig. S2F) raise the possibility that, these three proteins like MeCP2, Sin3A, and HDAC2 may constitute a multiprotein co-repressor complex, i.e., MeCP2/Sin3A/HDAC2 corepressor complex, to function in the transcriptional regulation of *kcnq2* and *kcnq3* genes. To test this understanding, we first examined the distribution of MeCP2, Sin3A and HDAC2 expression in cultured DRG neurons using immunofluorescent staining, and found an evident co-localization of MeCP2, Sin3A, and HDAC2 in the DRG neurons (Fig. S9A). Next, we explored the effects of knockdown Sin3A on the enrichment of MeCP2/HDAC2 corepressor complex in the *kcnq2* and *kcnq3* genes promoter of BCP model rats. Knockdown of Sin3A in DRG neurons was carried out by intrathecal administration of Sin3A siRNA (2.5 μg in a 10-μl volume) to BCP model rats on day 7 after tumor cells inoculation, twice per day for seven consecutive days, and the following biochemical analyses and behavioral test were respectively performed on day 14 after tumor cells inoculation. The results showed that the elevated expression of Sin3A mRNA level was significantly decreased in ipsilateral L4/5 DRG tissues of Sin3A siRNA-treated rats (Fig. S9B), validating that intrathecal Sin3A siRNA could effectively knock down Sin3A in the DRG neurons. Along with the knockdown of Sin3A in DRG neurons, a significant decrease in relative enrichment of MeCP2/HDAC2 corepressor complex was observed in the *kcnq2* and *kcnq3* genes promoter of DRG neurons in BCP model rats (Fig. S9C and D), indicating an impaired binding of MeCP2/HDAC2 corepressor in the *kcnq2* and *kcnq3* genes promoter of DRG neurons in BCP model rats that received

(See figure on next page.)

Fig. 3 Knockdown of MeCP2 in DRG neurons impairs HDAC2-mediated transcriptional repression of *kcnq2* and *kcnq3* genes, reduces the neuronal excitability and attenuates pain hypersensitivity in bone cancer pain model rats. (**A**-**F**) ChIP-qPCR assays for the enrichment of MeCP2-HDAC2 complex, acetylated histone 3 (H3Kac) and acetylated histone 4 (H4Kac) in the *kcnq2* and *kcnq3* genes promoter, in ipsilateral L4/5 DRG tissues obtained from bone cancer pain (BCP) model rats that received intrathecal LV-shMeCP2 or the control LV-ZsGreen, performed at 14 days after tumor cells inoculation. (**A** and **B**) for MeCP2-HDAC2 complex ($n = 6$–8 rats per group); (**C** and **D**) for H3Kac ($n = 6$–8 rats per group); (**E** and **F**) for H4Kac ($n = 6$–7 rats per group). (**G**-**J**) RT-qPCR and Western blot analyses of the mRNA and protein abundance of KCNQ2 and KCNQ3 in ipsilateral L4/5 DRG tissues obtained from BCP model rats that received intrathecal LV-shMeCP2 or LV-ZsGreen, performed at 14 days after tumor cells inoculation. (**G** and **H**) for KCNQ2, (**I** and **J**) for KCNQ3, $n = 5$–7 rats per group. Upper in (**H** and **J**): Representative blots are shown. (**K**-**Q**) Electrophysiological analyses of M-currents (**K** and **O**) and neuronal excitability (**L**-**Q**) in ipsilateral L4/5 DRG neurons of BCP model rats that received intrathecal LV-shMeCP2 or LV-ZsGreen, recorded at 14 days after tumor cells inoculation. (**K** and **L**) Representative traces of M-currents (**K**) and neuronal action potentials (**L**) evoked by a large depolarizing current pulse (1-s, 2-fold AP rheobase) are shown. Scale bar = 100 pA, 300 ms for (**K**), and 20 mV, 100 ms for (**L**). (**M** and **N**) Analysis of neuronal firing rate (spikes/second) elicited by a series of 500-ms depolarizing current pulses (in 50-pA steps from 0 to 400 pA). (**M**) Representative traces of evoked action potentials (APs) by 100 pA, 200 pA, and 300 pA depolarizing current pulses are shown. Scale bar = 20 mV, 200 ms. (**O**-**Q**) Plots of M-current density, frequency of APs, inter-spike intervals (ISI), AP amplitude, after hyperpolarization (AHP) amplitude, $AHP_{80\%}$ duration (**O**), threshold potential (**P**), and rheobase (**Q**) ($n = 20$–30 cells from six rats per group). (**R** and **S**) Assessment of ipsilateral PWT (**R**) and PWL (**S**) for BCP model rats that received intrathecal LV-shMeCP2 or LV-ZsGreen, performed at 14 days after tumor cells inoculation ($n = 13$–14 rats per group). (**T**) Assessment of animal's locomotor function before and after intrathecal lentivirus administration ($n = 13$–14 rats per group). Data are presented as mean ± SEM. $^{*}p < 0.05$, $^{**}p < 0.01$, $^{***}p < 0.001$, unpaired *t* test for (**A**)-(**J**) and (**O**)-(**Q**); two-way ANOVA with Sidak's *post hoc* test for (**N**) and (**R**)-(**T**). See also Fig. S7-S9

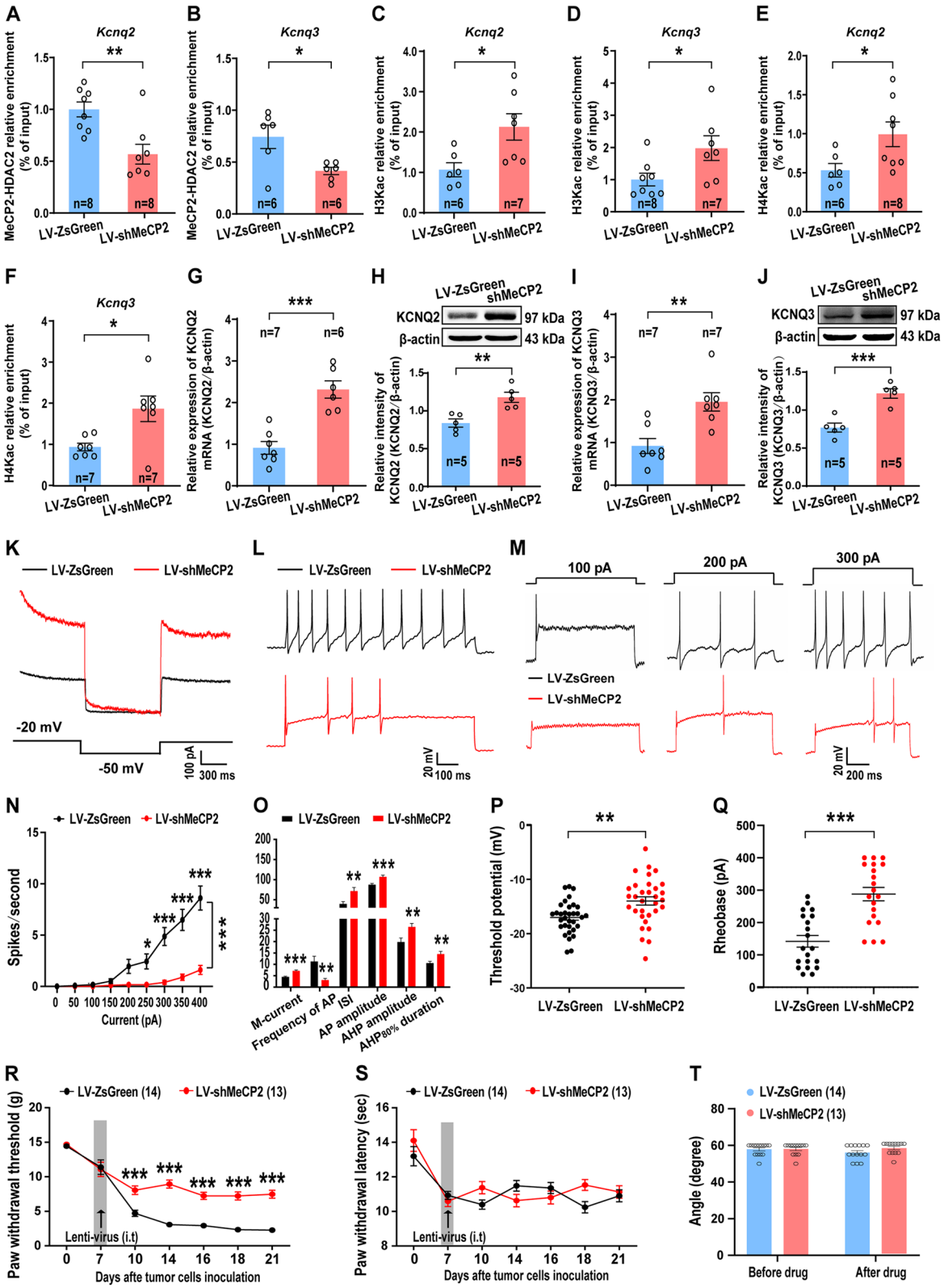

Fig. 3 (See legend on previous page.)

intrathecal Sin3A siRNA. Correspondingly, the behavioral tests showed that the mechanical hypersensitivity, assessed by the decreased PWT in response to von Frey filaments stimuli, was alleviated in BCP model rats treated with intrathecal Sin3A siRNA compared to the scramble control (Fig. S9E). Moreover, the results from inclined-plate test revealed that the animal's locomotor function was not impaired after intrathecal siRNA application (Fig. S9F). These data indicate that knockdown of Sin3A in DRG neurons disrupts the binding of MeCP2/HDAC2 corepressor in the *kcnq2* and *kcnq3* genes promoter of DRG neurons, subsequently rescues the transcriptional repression of Kv7(KCNQ)/M potassium channels in DRG neurons and the pathology of BCP in tumor-bearing rats, supporting our understanding that the formation of MeCP2/Sin3A/HDAC2 corepressor complex by the link of MeCP2 and HDAC2 through Sin3A, is required for the transcriptional repression of Kv7(KCNQ)/M potassium channels in DRG neurons and the pathogenesis of BCP in tumor-bearing rats with bone metastasis (Fig. S9G).

Contribution of EREG to HDAC2-mediated transcriptional repression of Kv7(KCNQ)/M potassium channels in DRG neurons and its role in bone cancer-induced pain in rats

Furthermore, we sought to explore the upstream signal molecules for the activation of HDAC2-mediated transcriptional repression of Kv7(KCNQ)/M potassium channels in the DRG neurons of BCP model rats. Data from KEGG enrichment analysis of the aforementioned RNA-seq showed that, the EGFR tyrosine kinase inhibitor resistance pathway, ErbB signaling pathway, Ras signaling pathway, and MAPK signaling pathway are activated in BCP model rats (Fig. 1A), and multiple potential genes including genes encoding potassium channel (*Kcnq, Kcnh, Kcnj, Kcnb*) and EGF family ligands and receptors (*Ereg, Egfr*), as well as *Mecp2*, *Sin3a*, *Mapk3*, *Runx1*, etc. are predicted be interconnected with *Hdac2* (Fig. S2G). It is well accepted that the EGF family ligands and receptors are implicated in cell proliferation, differentiation, division, survival, and cancer development [46, 47]. The EGF family of ligands includes eleven structurally related proteins, namely EGF, transforming growth factor a (TGF-α), amphiregulin (AREG), epigen (EPGN), heparin-binding EGF-like growth factor (HB-EGF), epiregulin (EREG), betacellulin (BTC), and the neuregulins (NRG1-4) [48]. The biological effects of the EGF family ligands are acted on through EGF receptor (EGFR) family that belongs to the ErbB receptor family of the Receptor Tyrosine Kinase superfamily (RTKs), including EGFR (also known as ErbB1), ErbB2, ErbB3 and ErbB4 four members [49], among those the role of EGFR in pain processing has been reported in many studies [50]. The downstream effects of EGFR are mediated by a number of signaling pathways including the Ras/ERK cascade [17, 51–53], which regulates multiple pain responses [54–57]. The activation of ERK signaling is implicated in the post-translational modifications, especially the phosphorylated modification of Runx1 [18, 19], a Runt domain transcription factor that is required for the differentiation of nociceptors and the pathogenesis of persistent pain [20, 21, 58, 59]. Also, Runx1 has been shown to transcriptionally regulate HDAC2 expression in breast cancer tissues [22]. To determine which member of the EGF family ligands is involved in HDAC2-mediated transcriptional repression of Kv7(KCNQ)/M potassium channels in the DRG neurons of BCP model rats, we first examined the alterations of both EGF and TGF-α, two members of the classical EGF family ligands, in DRG neurons of BCP model rats. Unexpectedly, no significant alteration was observed on the mRNA expression of both EGF and TGF-α in ipsilateral L4/5 DRG tissues of BCP model rats (Fig. 4A and B). However, with respect to epiregulin (EREG), another member of the EGF family ligands that is involved in pain processing [16, 60, 61], a prominent increase in the abundance of both mRNA and protein levels, was found in ipsilateral L4/5 DRG tissues of BCP model rats (Fig. 4C and D), raising the possibility that EREG may be an upstream signal molecule for the activation of HDAC2-mediated transcriptional repression of Kv7(KCNQ)/M potassium channels in the DRG neurons of BCP model rats. To prove this speculation, we examined the effects of intrathecal EREG on the activation of HDAC2-mediated transcriptional repression of Kv7(KCNQ)/M potassium channels in the DRG neurons of naïve rats. EREG (50 μg/ml, 10 μl) or vehicle was intrathecally administered to naïve rats, once per day for four consecutive days, and the following behavioral tests, biochemical analyses and electrophysiological recordings were respectively performed on day 5 after drug application. The results showed that intrathecal EREG induced a statistical increase in the abundance of both phosphorylated ERK1/2 (pERK1/2) and phosphorylated Runx1 at serine 249 (pRunx1^{Ser249}) in the DRG neurons of naïve rats, while the abundance of total ERK1/2 protein and total Runx1 protein was not significantly altered after intrathecal EREG application (Fig. 4E-H). Meanwhile, immunofluorescence staining using antibody specific to Runx1 revealed that the nuclear localization of Runx1 (the colocalization of Runx1 and the nuclear marker DAPI) was significantly increased at 30 min after incubation of exogenous EREG (5 μl for 30 min) with 3 days-in-vitro (DIV) cultured rat DRG neurons (Fig. 4I), indicating that EREG activates a nuclear translocation of Runx1 in the DRG neurons. Runx1 is a Runt domain transcription factor that has been shown to transcriptionally regulate

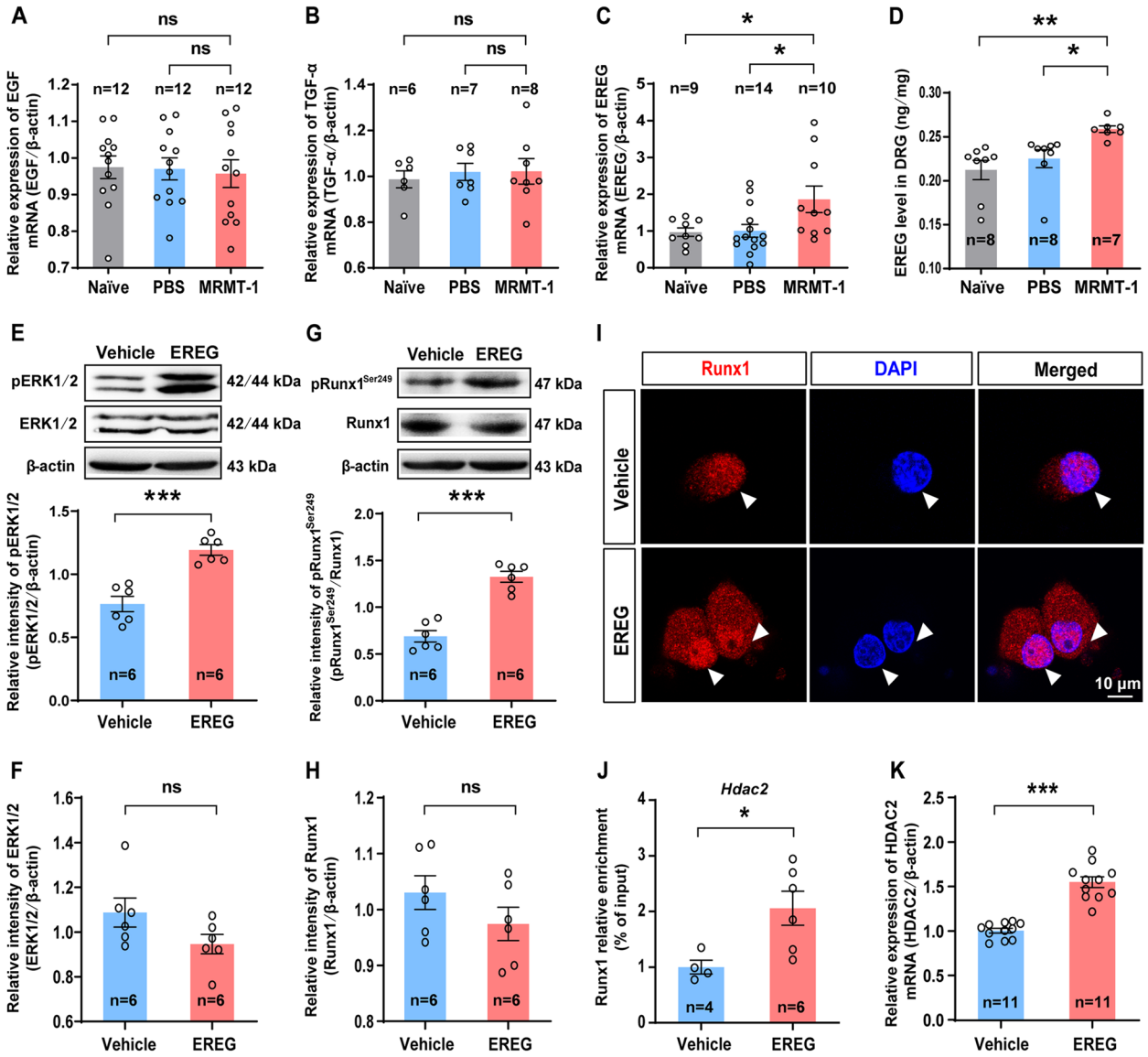

Fig. 4 Enhancement of epiregulin (EREG) in DRG neurons of bone cancer pain model rats and contribution of EREG to the activation of ERK-Runx1 signaling and upregulation of HDAC2 in DRG neurons. (**A**-**D**) Identification of EGF, TGF-α, and EREG mRNA levels by RT-qPCR analysis (**A**-**C**), and EREG protein abundance by ELISA (**D**), in ipsilateral L4/5 DRG tissues obtained from naïve, PBS-, and MRMT-1-treated rats, performed at 14 days after surgery ($n = 6$–12 rats per group). (**E**–**H**) Western blot analysis of phosphorylated ERK1/2 (pERK1/2, **E**), ERK1/2 (**F**), phosphorylated Runx1 at serine 249 site (pRunx1^{Ser249}, **G**), and Runx1 (**H**) protein abundance in L4/5 DRG tissues obtained from naïve rats that received intrathecal EREG or vehicle ($n = 6$ rats per group). Upper in (**E** and **G**): Representative blots are shown. (**I**) Representative images show the immunofluorescence with Runx1 (red) and DAPI (blue) in cultured rat DRG neurons at 30 min after incubation of exogenous EREG or vehicle. Right: merged images. Scale bar = 10 μm. (**J**) ChIP-qPCR assays for the enrichment of Runx1 in the *hdac2* gene promoter in L4/5 DRG tissues obtained from naïve rats that received intrathecal EREG or vehicle ($n = 4$–6 rats per group). (**K**) RT-qPCR analysis of HDAC2 mRNA level in L4/5 DRG tissues obtained from naïve rats that received intrathecal EREG or vehicle ($n = 11$ rats per group). Data are presented as mean ± SEM. $^{*}p < 0.05$, $^{**}p < 0.01$, $^{***}p < 0.001$; ns, not significant, one-way ANOVA followed by Dunnett's *post hoc* test for (**A**)-(**D**), unpaired *t* test for (**E**)-(**K**)

HDAC2 expression in breast cancer tissues [22]. In fact, a significant increase in relative enrichment of Runx1 was seen in the *hdac2* gene promotor of DRG neurons in rats received intrathecal EREG administration (Fig. 4J), suggesting that intrathecal EREG promotes an enhanced binding of Runx1 to *hdac2* gene promotor of DRG neurons in naïve rats. Correspondingly, the relative expression of HDAC2 at mRNA level was substantially increased in the DRG tissues of intrathecal EREG-treated naïve rats (Fig. 4K), implying the Runx1-mediated

transcriptional enhancement of HDAC2 in the DRG neurons of rats received intrathecal EREG application. Along with the enhanced expression of HDAC2 mRNA in the DRG neurons, a significant decrease in the abundance of KCNQ2 and KCNQ3 expression, at both mRNA and protein levels, was found in the DRG neurons of rats received intrathecal EREG application (Fig. 5A-D). Similarly, a reduced M-current density (2.35 ± 0.17 pA/pF EREG *vs.*

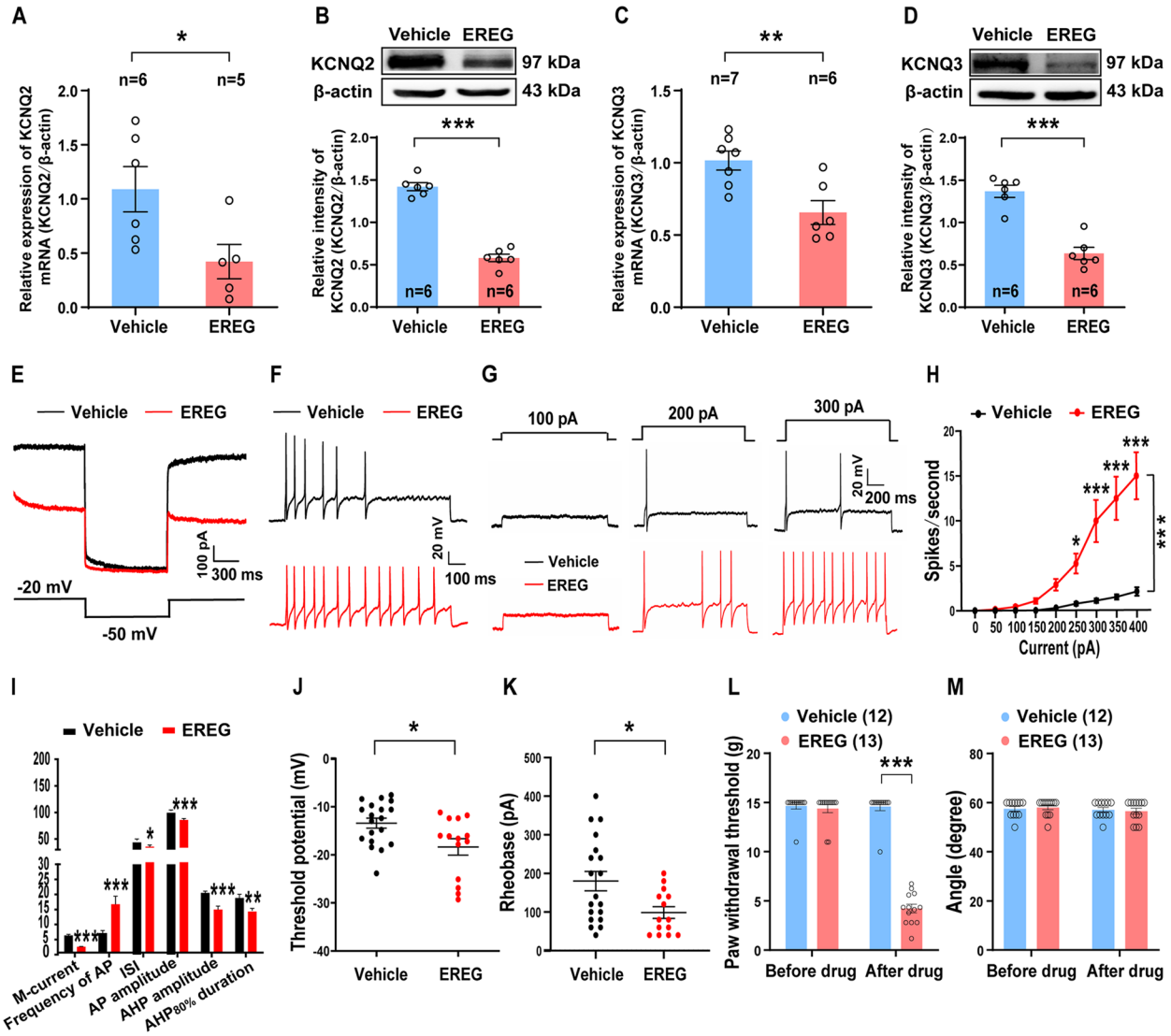

Fig. 5 Epiregulin (EREG) mediates *kcnq2* and *kcnq3* genes transcriptional repression in DRG neurons, enhances neuronal excitability and induces pain hypersensitivity in naïve rats. (**A**) RT-qPCR and Western blot analyses of the mRNA and protein abundance of KCNQ2 and KCNQ3 in L4/5 DRG tissues obtained from naïve rats that received intrathecal EREG or vehicle, performed at 5 days after drug administration. (**A** and **B**) for KCNQ2 ($n = 5$–6 rats per group); (**C** and **D**) for KCNQ3 ($n = 6$–7 rats per group). Upper in (**B** and **D**): Representative blots are shown. (**E**-**K**) Electrophysiological analyses of M-currents (**E** and **I**) and neuronal excitability (**F**-**K**) in L4/5 DRG tissues obtained from naïve rats that received intrathecal EREG or vehicle, recorded at 5 days after drug administration. (**E** and **F**) Representative traces of M-currents (**E**) and neuronal action potentials (**F**) evoked by a large depolarizing current pulse (1-s, 2-fold AP rheobase) are shown. Scale bar = 100 pA, 300 ms for (**E**), and 20 mV, 100 ms for (**F**). (**G** and **H**) Analysis of neuronal firing rate (spikes/second) elicited by a series of 500-ms depolarizing current pulses (in 50-pA steps from 0 to 400 pA). (**G**) Representative traces of evoked action potentials (APs) by 100 pA, 200 pA, and 300 pA depolarizing current pulses are shown. Scale bar = 20 mV, 200 ms. (**I**-**K**) Plots of M-current density, frequency of APs, inter-spike intervals (ISI), AP amplitude, after hyperpolarization (AHP) amplitude, $AHP_{80\%}$ duration (**I**), threshold potential (**J**), and rheobase (**K**) ($n = 20$–30 cells from six rats per group). (**L**) Assessment of the PWT for naive rats that received intrathecal EREG or vehicle, performed at 5 days after drug administration ($n = 12$–13 rats per group). (**M**) Assessment of animal's locomotor function before and after intrathecal drug administration ($n = 12$–13 rats per group). Data are presented as mean ± SEM. $^{*}p < 0.05$, $^{**}p < 0.01$, $^{***}p < 0.001$, unpaired *t* test for (**A**)-(**D**) and (**I**-**K**); two-way ANOVA with Sidak's *post hoc* test for (**H**), (**L**), and (**M**)

5.61 ± 0.34 pA/pF vehicle, $P < 0.0001$), an enhanced neuronal excitability including the increase of action potential (AP) frequency, the decreases of inter-spike intervals (ISI), AP amplitude, after hyperpolarization (AHP) amplitude, $AHP_{80\%}$ duration, the threshold potential and rheobase, were seen in the DRG neurons of rats treated with intrathecal EREG (Fig. 5E-K). Besides, the behavioral test revealed that intrathecal administration of EREG to rats produced evident mechanical hypersensitivity that was assessed by the decreased PWT in response to von Frey filaments stimuli (Fig. 5L). The results from inclined-plate test revealed that the animal's locomotor function was not impaired after intrathecal EREG treatment (Fig. 5M). These results suggest that EREG may be an upstream signal molecule involved in HDAC2-mediated transcriptional repression of Kv7(KCNQ)/M potassium channels in the DRG neurons of BCP model rats, via the activation of ERK-Runx1 signaling pathway.

Contribution of EGFR to HDAC2-mediated transcriptional repression of Kv7(KCNQ)/M potassium channels in DRG neurons and its role in bone cancer-induced pain in rats

EREG is a 46-amino acid protein in the EGF family that binds to the following 4 different receptors: the EGFR and human EGF receptor 2, 3, or 4 (HER 2, 3, or 4; in rodents referred to as ErbB 2, 3, or 4, respectively). Earlier observations show that EREG induces intracellular signaling mainly through EGFR or HER4 [62]. Manipulation of the EREG signaling with blocking one of its receptors (i.e. EGFR) may reduce neuropathic pain [63], while activation of the EGFR by EREG enhances pain [16, 60]. To further determine whether EREG acts through EGFR to modulate the HDAC2-mediated transcriptional repression of Kv7(KCNQ)/M potassium channels in DRG neurons and its role in bone cancer-induced pain in rats, we first examined the expression and distribution of EGFR in the DRG neurons. As expected, an evident co-localization of EGFR with HDAC2 and KCNQ2/KCNQ3 was found in cultured rat DRG neurons (Fig. S10A), and also, the EGFR was widely expressed in $NF200^+$-, $CGRP^+$-, and $IB4^+$-DRG neurons across the naïve, PBS, and MRMT-1 rats (Fig. S10B-D). The mean fluorescence intensity of EGFR was significantly increased in all these three types of DRG neurons in BCP model rats compared to the naïve and PBS controls (Fig. S10E-G). Besides, a significant increase in the abundance of EGFR expression, at both protein and mRNA levels, was found in ipsilateral L4/5 DRG tissues of BCP model rats compared to the naïve and PBS controls (Fig. S10H and I). Furthermore, we investigated whether EGFR inhibition could rescue the transcriptional repression of Kv7(KCNQ)/M channels in DRG neurons and the pain hypersensitivity in BCP model rats. AG1478 (50 μM × 10 μl), a selective EGFR inhibitor, was delivered intrathecally to BCP model rats on day 10 after tumor cells inoculation, once per day for four consecutive days. The results revealed that intrathecal AG1478 effectively reversed the decreased expression of KCNQ2 and KCNQ3 submits encoding Kv7(KCNQ)/M channels, at both mRNA and protein levels, in ipsilateral L4/5 DRG tissues of bone metastasis model rats (Fig. S10J-M). Meanwhile, the tumor-induced pain hypersensitivity, as assessed by the decreases of paw withdrawal threshold (PWT) in response to von Frey filaments stimuli and paw withdrawal latency (PWL) in response to radiant heat stimulation, was significantly alleviated by intrathecal AG1478 application to MRMT-1 tumor-bearing rats (Fig. S10N and O). Also, the results from inclined-plate test revealed that the animal's locomotor function was not impaired after intrathecal AG1478 administration (Fig. S10P). These findings raise the possibility that the upregulated EGFR in DRG neurons probably involves in the transcriptional repression of *kcnq2* and *kcnq3* genes and the pathogenesis of BCP in bone metastasis model rats.

Next, we determined the involvement of EGFR in EREG-induced activation of ERK-Runx1 signaling cascade as well as in HDAC2-mediated transcriptional repression of Kv7(KCNQ)/M potassium channels in DRG neurons and its role in bone cancer-induced pain in rats, by investigating the effects of knockdown EGFR in DRG neurons on the aforementioned actions of intrathecal EREG to naïve rats. Knockdown of EGFR in DRG neurons was performed by intrathecal administration of lentivirus expressing EGFR shRNA linked with ZsGreen (LV-shEGFR) to rats, and the efficiency of knockdown EGFR in DRG neurons was validated by immunofluorescence staining, RT-qPCR and Western blotting analysis from either cultured rat DRG neurons at 48 h after transfected with LV-shEGFR (Fig. S11A-D), or the DRG tissues of rats on day 7 after received intrathecal lentivirus application (Fig. S11E-H). The results showed that knockdown EGFR in DRG neurons could effectively abrogate the intrathecal EREG-induced upregulation of both pERK1/2 (Fig. S12A-C) and $pRunx1^{Ser249}$ (Fig. S12D-F) protein in the DRG neurons of EREG-treated rats. Moreover, the increased abundance of HDAC2 protein (Fig. S12G), and the decreased abundance of KCNQ2 and KCNQ3 proteins (Fig. S12H and I), induced by intrathecal EREG to rats, were significantly restored by knocking-down EGFR in DRG neurons. Also, the augmented pain hypersensitivity in intrathecal EREG-treated rats, indicated by decreased PWT in response to von Frey filaments stimuli, was rescued by knocking-down EGFR in DRG neurons (Fig. S12J), while the animal's locomotor function was not impaired after intrathecal lentivirus administration (Fig. S12K). These data demonstrate the necessary of

EGFR for EREG-induced activation of ERK-Runx1 signaling and the HDAC2-mediated transcriptional repression of Kv7(KCNQ)/M potassium channels in the DRG neurons of intrathecal EREG-treated rats.

Furthermore, we investigated whether EGFR is involved in the activation of ERK-Runx1 signaling and the HDAC2-mediated transcriptional repression of Kv7(KCNQ)/M potassium channels in DRG neurons of BCP model rats. Our results revealed that using intrathecal LV-shEGFR to knock down EGFR in the DRG neurons of BCP model rats, it significantly rescued the increased abundance of both pERK1/2 (Fig. S13A-C) and pRunx1^{Ser249} (Fig. S13D-F) protein in ipsilateral L4/5 DRG tissues of tumor-bearing rats, indicating the involvement of EGFR in the activation of ERK-Runx1 signaling in BCP model rats. Moreover, accompanied with the knockdown of EGFR in DRG neurons, a significant decrease in the abundance of HDAC2 expression, at both mRNA and protein levels, was observed in ipsilateral L4/5 DRG tissues of BCP model rats that received intrathecal LV-shEGFR application (Fig. 6A and B). Correspondingly, the relative enrichment of HDAC2 in the *kcnq2* and *kcnq3* genes promoter was significantly decreased (Fig. 6C and D), and the enrichment of both H3Kac and H4Kac in the *kcnq2* and *kcnq3* genes promoter was statistically increased (Fig. 6E-H), in ipsilateral L4/5 DRG tissues of BCP model rats treated with intrathecal LV-shMeCP2 compared to the control LV-ZsGreen. In line with these findings, a substantially increase in the abundance of KCNQ2 and KCNQ3 expression, at both mRNA and protein levels, was seen in ipsilateral L4/5 DRG tissues obtained from BCP model rats that received intrathecal LV-shEGFR application (Fig. 6I-L). As a result, the M-current density was increased (9.29 ± 0.70 pA/pF EREG *vs.* 4.70 ± 0.31 pA/pF vehicle, $P < 0.0001$), whereas the neuronal excitability was reduced (inferred from the intrinsic electrogenic properties, including the decreased AP frequency as well as the increased ISI, AP amplitude, AHP amplitude, $AHP_{80\%}$ duration, the threshold potential and rheobase), in ipsilateral L4/5 DRG neurons of BCP model rats that received intrathecal LV-shEGFR relative to the control LV-ZsGreen (Fig. 6M-Q). Also, both of the mechanical hypersensitivity (assessed by the decreased PWT in response to von Frey filaments stimuli) and the thermal hyperalgesia (assessed by the reduced PWL in response to radiant heat stimulation) were alleviated in the BCP model rats that received intrathecal LV-shEGFR application (Fig. 6R and S). The results from inclined-plate test revealed that the animal's locomotor function was not impaired after intrathecal lentivirus treatment (Fig. 6T). These data indicate that knockdown EGFR by intrathecal LV-shEGFR effectively restores the activation of ERK-Runx1 signaling and the HDAC2-mediated transcriptional repression of Kv7(KCNQ)/M channels in DRG neurons of BCP model rats, subsequently reduces the neuronal hyperexcitability and pain hypersensitivity in tumor-bearing rats, supporting the roles of EGFR in HDAC2-mediated transcriptional repression of Kv7(KCNQ)/M potassium channels in DRG neurons and the pathogenesis of BCP in tumor-bearing rats.

(See figure on next page.)

Fig. 6 Knockdown of EGFR in DRG neurons impairs HDAC2-mediated transcriptional repression of *kcnq2* and *kcnq3* genes, reduces neuronal excitability and attenuates pain hypersensitivity in bone cancer pain model rats. (**A** and **B**) RT-qPCR and Western blot analyses of HDAC2 mRNA (**A**) and protein (**B**) abundance in ipsilateral L4/5 DRG tissues obtained from bone cancer pain (BCP) model rats that received intrathecal LV-shEGFR or the control LV-ZsGreen, performed at 14 days after tumor cells inoculation ($n = 6$–8 rats per group). Upper in (**B**): Representative blots are shown. (**C**-**H**) ChIP-qPCR assays for the enrichment of HDAC2, acetylated histone 3 (H3Kac), and acetylated histone 4 (H4Kac) in the *kcnq2* and *kcnq3* genes promoter, in ipsilateral L4/5 DRG tissues obtained from bone cancer pain (BCP) model rats that received intrathecal LV-shEGFR or the control LV-ZsGreen, performed at 14 days after tumor cells inoculation. (**C** and **D**) for HDAC2 ($n = 5$–6 rats per group); (**E** and **F**) for H3Kac ($n = 5$ rats per group); (**G** and **H**) for H4Kac ($n = 5$–6 rats per group). (**I**-**L**) RT-qPCR and Western blot analyses of the mRNA and protein abundance of KCNQ2 and KCNQ3 in ipsilateral L4/5 DRG tissues obtained from BCP model rats that received intrathecal LV-shEGFR or LV-ZsGreen, performed at 14 days after tumor cells inoculation. (**I** and **J**) for KCNQ2 ($n = 6$–7 rats per group); (**K** and **L**) for KCNQ3 ($n = 5$–7 rats per group). Upper in (**J** and **L**): Representative blots are shown. (**M**-**Q**) Electrophysiological analyses of M-currents (**M** and **O**) and neuronal excitability (**N**-**Q**) in ipsilateral L4/5 DRG neurons of BCP model rats that received intrathecal LV-shEGFR or LV-ZsGreen, recorded at 14 days after tumor cells inoculation. (**M** and **N**) Representative traces of M-currents (**M**) and neuronal action potentials (**N**) evoked by a large depolarizing current pulse (1-s, 2-fold AP rheobase) are shown. Scale bar = 100 pA, 300 ms for (**M**), and 20 mV, 100 ms for (**N**). (**O**-**Q**) Plots of M-current density, frequency of APs, inter-spike intervals (ISI), AP amplitude, after hyperpolarization (AHP) amplitude, $AHP_{80\%}$ duration (**O**), threshold potential (**P**), and rheobase (**Q**) ($n = 20$–30 cells from six rats per group). (**R** and **S**) Assessment of ipsilateral PWT (**R**) and PWL (**S**) for BCP model rats that received intrathecal LV-shEGFR or LV-ZsGreen, performed at 14 days after tumor cells inoculation ($n = 11$–12 rats per group). (**T**) Assessment of animal's locomotor function before and after intrathecal lentivirus administration ($n = 11$–12 rats per group). Data are presented as mean ± SEM. $^{*}p < 0.05$, $^{**}p < 0.01$, $^{***}p < 0.001$, unpaired *t* test for (**A**)-(**L**) and (**O**)-(**Q**); two-way ANOVA with Sidak's *post hoc* test for (**R**)-(**T**). See also Fig. S10-S13

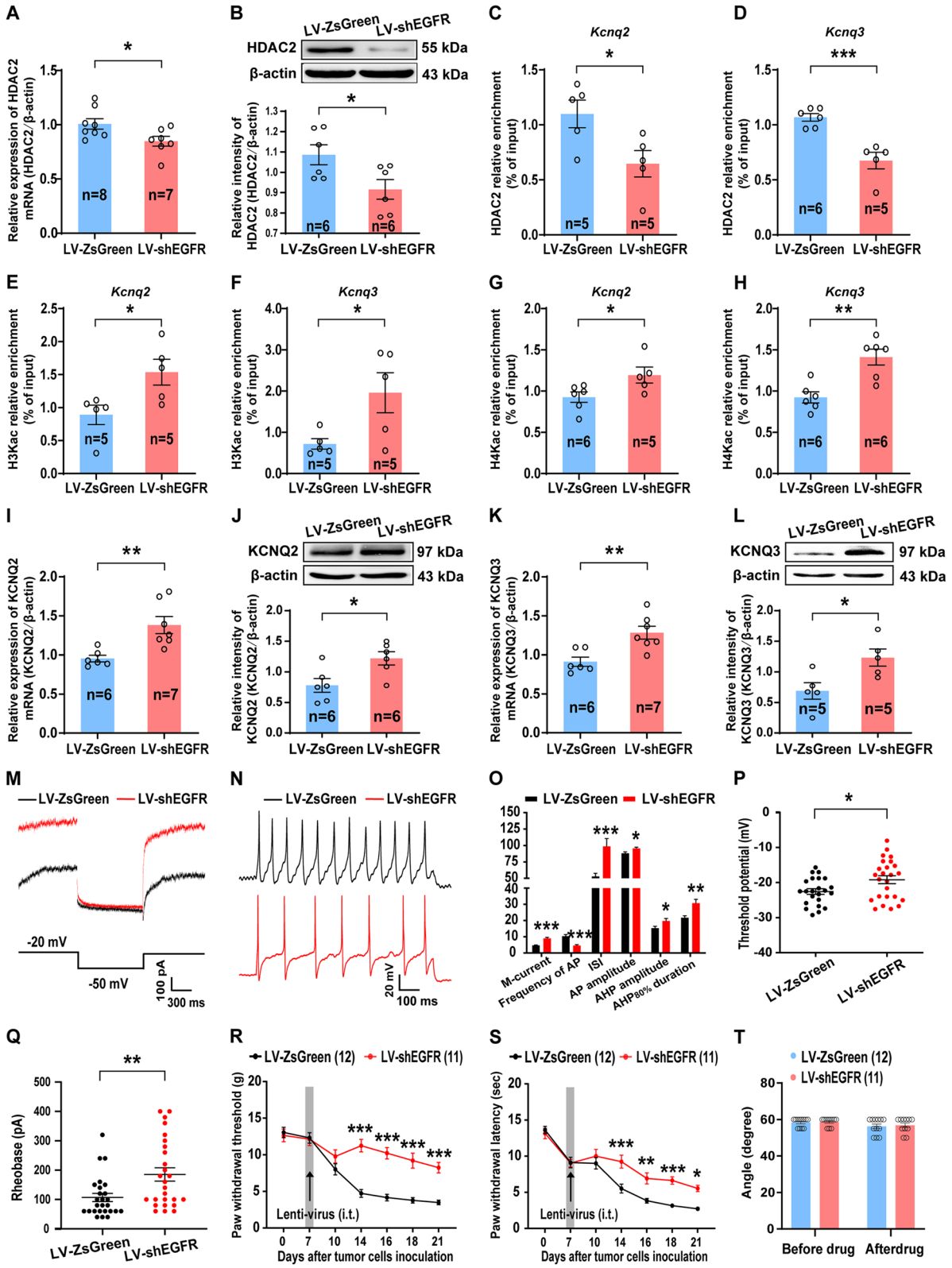

Fig. 6 (See legend on previous page.)

Involvement of ERK-Runx1 signaling cascade in HDAC2-mediated transcriptional repression of Kv7(KCNQ)/M potassium channels in DRG neurons and its role in bone cancer-induced pain in rats

As mentioned above, the ERK-Runx1 signaling cascade is a downstream target for the activation of EREG/EGFR signaling [17–19, 51–53], and the Runx1 is found to serve as a transcriptional regulator of HDAC2 in breast cancer tissues [22]. Our RNA-seq data, both of the KEGG enrichment analysis and the DEGs' gene–gene interaction networks analysis for HDAC2, also predicted a potential interaction of ERK-Runx1 signaling for HDAC2 (Fig. 1A, Fig. S2F and G). With interrupting the ERK-Runx1 signaling pathway by ERK inhibitor (SCH772984) or Runx1 siRNA, we indeed found that either intrathecal administration of SCH772984 (15 μM × 10 μl) to inhibit ERK activation, or intrathecal application of Runx1 siRNA (2.5 μg in a 10-μl volume) to knock down Runx1 in the DRG neurons, could rescue intrathecal EREG-induced increase of HDAC2 protein abundance, and as well, restore intrathecal EREG-induced reduction of KCNQ2 and KCNQ3 protein levels, in the DRG tissues of EREG-treated rats (Fig. S14A-F). Similarly, both SCH772984 and Runx1 siRNA could effectively abrogate intrathecal EREG-induced pain hypersensitivity but did not impair the animal's locomotor function in EREG-treated rats (Fig. S14G-J). These results support our understanding that the ERK-Runx1 signaling cascade is indeed a downstream target for EREG-induced upregulation of HDAC2 expression, subsequently contributing to HDAC2-mediated transcriptional repression of Kv7(KCNQ)/M channels in DRG neurons and pain hypersensitivity in EREG-treated rats.

To further determine whether the activation of ERK-Runx1 signaling in DRG neurons is involved in HDAC2-mediated transcriptional repression of Kv7(KCNQ)/M potassium channels in DRG neurons and the development of BCP in tumor-bearing rats, we then examined the effects of either inhibiting ERK activation or knockdown Runx1 on HDAC2-mediated transcriptional repression of *kcnq2* and *kcnq3* genes, and as well, on the pathogenesis of BCP in MRMT-1 tumor-bearing rats. The ERK inhibitor SCH772984 (15 μM × 10 μl) was intrathecally administered to tumor-bearing rats on day 7 after tumor cells inoculation, twice per day for seven consecutive days, and the following biochemical analysis and electrophysiological recordings were respectively performed on day 14 after tumor cells inoculation. The results showed that intrathecal administration of the ERK inhibitor SCH772984 significantly reduced the abundance of pRunx1^{Ser249} in ipsilateral L4/5 DRG tissues of tumor-bearing rats (Fig. 7A and B), indicating that the phosphorylated modification of Runx1 in DRG neurons is dependent upon the activation of ERK signaling in BCP model rats. Moreover, inhibition of ERK action by intrathecal SCH772984 also reduced the relative enrichment of Runx1 in *hdac2* gene promotor of DRG neurons (Fig. 7C) and the abundance of HDAC2 protein in ipsilateral L4/5 DRG tissues of BCP model rats (Fig. 7D), validating that the Runx1 is indeed a transcriptional regulator of HDAC2 in the DRG neurons of tumor-bearing rats [22]. In agreement with the reduction of HDAC2

(See figure on next page.)

Fig. 7 Inhibition of ERK signaling impairs Runx1-dependent upregulation of HDAC2 and HDAC2-mediated transcriptional repression of *kcnq2* and *kcnq3* genes, reduces neuronal excitability and attenuates pain hypersensitivity in bone cancer pain model rats. (**A** and **B)** Western blot analysis of phosphorylated Runx1 at serine 249 (pRunx1^{Ser249}) (**A**) and Runx1 (**B**) protein abundance in ipsilateral L4/5 DRG tissues obtained from BCP model rats that received intrathecal SCH772984 (a selective ERK inhibitor), performed at 14 days after tumor cells inoculation ($n = 5$ rats per group). Upper in (**A**): Representative blots are shown. (**C**) ChIP-qPCR assays for the enrichment of Runx1 in *hdac2* gene promoter, in ipsilateral L4/5 DRG tissues obtained from bone cancer pain (BCP) model rats that received intrathecal SCH772984 or vehicle, performed at 14 days after tumor cells inoculation ($n = 4$–5 rats per group). (**D**) Western blot analysis of HDAC2 protein abundance in ipsilateral L4/5 DRG tissues obtained from BCP model rats that received intrathecal SCH772984 or vehicle, performed at 14 days after tumor cells inoculation ($n = 6$ rats per group). Upper: Representative blots are shown. (**E**–**H**) RT-qPCR and Western blot analyses of the mRNA and protein abundance of KCNQ2 and KCNQ3 in ipsilateral L4/5 DRG tissues obtained from BCP model rats that received intrathecal SCH772984 or vehicle, performed at 14 days after tumor cells inoculation. (**E** and **F**) for KCNQ2 ($n = 6$ rats per group); (**G** and **H**) for KCNQ3 ($n = 6$–7 rats per group). Upper in (**F** and **H**): Representative blots are shown. (**I**-**O**) Electrophysiological analyses of M-currents (**I** and **M**) and neuronal excitability (**J**-**O**) in ipsilateral L4/5 DRG neurons of BCP model rats that received intrathecal SCH772984 or vehicle, recorded at 14 days after tumor cells inoculation. (**I** and **J**) Representative traces of M-currents (**I**) and neuronal action potentials (**J**) evoked by a large depolarizing current pulse (1-s, 2-fold AP rheobase) are shown. Scale bar = 100 pA, 300 ms for (**I**), and 20 mV, 100 ms for (**J**). (**K** and **L**) Analysis of neuronal firing rate (spikes/second) elicited by a series of 500-ms depolarizing current pulses (in 50-pA steps from 0 to 400 pA). (**K**) Representative traces of evoked action potentials (APs) by 100 pA, 200 pA, and 300 pA depolarizing current pulses are shown. Scale bar = 20 mV, 200 ms. (**M**–**O**) Plots of M-current density, frequency of APs, inter-spike intervals (ISI), AP amplitude, after hyperpolarization (AHP) amplitude, $AHP_{80\%}$ duration (**M**), threshold potential (**N**), and rheobase (**O**) ($n = 20$–30 cells from six rats per group). (**P**) Assessment of ipsilateral PWT for BCP model rats that received intrathecal SCH772984 or vehicle, performed at 14 days after tumor cells inoculation ($n = 10$ rats per group). (**Q**) Assessment of animal's locomotor function before and after intrathecal drug administration ($n = 10$ rats per group). Data are presented as mean ± SEM. $^{*}p < 0.05$, $^{**}p < 0.01$, $^{***}p < 0.001$; ns, not significant, unpaired *t* test for (**A**)-(**H**) and (**M**)-(**O**); two-way ANOVA with Sidak's *post hoc* test for (**L**), (**P**), and (**Q**). See also Fig. S14-15

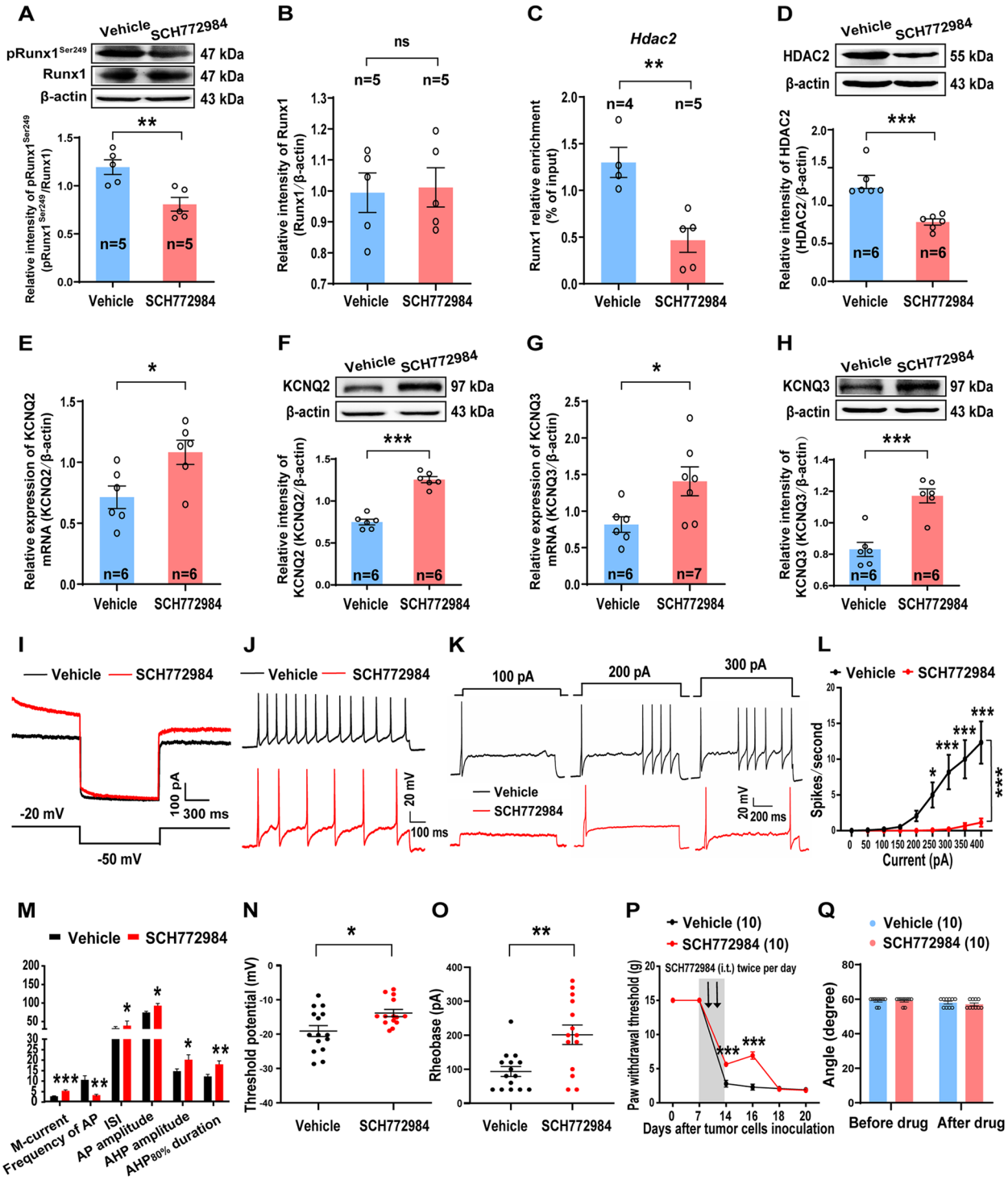

Fig. 7 (See legend on previous page.)

protein level, a significant decrease in the abundance of KCNQ2 and KCNQ3 expression in ipsilateral L4/5 DRG tissues, at both mRNA and protein levels, was found in BCP model rats treated with intrathecal SCH772984 compared to the vehicle controls (Fig. 7E-H). Also, the M-current density was increased (5.40 ± 0.46 pA/pF SCH772984 *vs.* 2.28 ± 0.17 pA/pF vehicle, $P < 0.0001$), whereas the neuronal excitability was reduced (inferred

from the intrinsic electrogenic properties, including the decreased AP frequency as well as the increased ISI, AP amplitude, AHP amplitude, $AHP_{80\%}$ duration, the threshold potential and rheobase), in ipsilateral L4/5 DRG neurons of BCP model rats treated with intrathecal SCH772984 (Fig. 7I-O). Correspondingly, the augmented pain hypersensitivity in bone metastasis model rats, indicated by decreased PWT in response to von Frey filaments stimuli, was abrogated by intrathecal administration of SCH772984 (Fig. 7P). The results from inclined-plate test revealed that the animal's locomotor function was not impaired after intrathecal SCH772984 administration (Fig. 7Q).

Likewise, knockdown of Runx1 in DRG neurons was performed by intrathecal administration of small interfering RNA (siRNA) targeting for Runx1 (Runx1 siRNA, 2.5 μg in a 10-μl volume) to bone metastasis model rats, twice per day for seven consecutive days on day 7 after tumor cells inoculation, and the following biochemical analysis and electrophysiological recordings were respectively performed on day 14 after tumor cells inoculation. The results showed that the abundance of Runx1 protein was significantly decreased in ipsilateral L4/5 DRG tissues of BCP model rats treated with intrathecal Runx1 siRNA (Fig. S15A), validating that intrathecal Runx1 siRNA could effectively knock down Runx1 in the DRG neurons. Along with the knockdown of Runx1 in DRG neurons, the relative enrichment of Runx1 in *hdac2* gene promotor of DRG neurons (Fig. S15B), and the abundance of HDAC2 mRNA and protein expression, were significantly decreased in ipsilateral L4/5 DRG tissues of bone metastasis model rats with intrathecal Runx1 siRNA treatment (Fig. S15C and D), demonstrating the role of Runx1 in the transcriptional regulation of HDAC2 in DRG neurons of tumor-bearing rats. In line with the downregulation of HDAC2 expression in DRG neurons, the abundance of KCNQ2 and KCNQ3 expression, at both mRNA and protein levels, was substantially increased in ipsilateral L4/5 DRG tissues of BCP model rats treated with intrathecal Runx1 siRNA (Fig. S15E-H). Also, the M-current density was increased (7.00 ± 0.68 pA/pF Runx1 siRNA *vs.* 3.23 ± 0.18 pA/pF scramble, $P < 0.0001$), whereas the neuronal excitability was reduced (inferenced by the intrinsic electrogenic properties, including the decreased AP frequency as well as the increased ISI, AP amplitude, AHP amplitude, $AHP_{80\%}$ duration, the threshold potential and rheobase), in ipsilateral L4/5 DRG neurons of BCP model rats treated with intrathecal Runx1 siRNA compared to the scramble controls (Fig. S15I-O). Correspondingly, the behavioral tests showed that the mechanical hypersensitivity (assessed by the decreased PWT in response to von Frey filaments stimuli) was alleviated in BCP model rats treated with intrathecal Runx1 siRNA (Fig. S15P, day 14 and day 16: $P < 0.0001$, Runx1 siRNA *vs.* scramble). Moreover, the results from inclined-plate test revealed that the animal's locomotor function was not impaired after intrathecal siRNA application (Fig. S15Q).

Taken together, these results suggest that disrupting the activation of EGFR-ERK-Runx1 signaling in DRG neurons abrogates the HDAC2-mediated transcriptional repression of *kcnq2* and *kcnq3* genes encoding Kv7(KCNQ)/M potassium channels, and reduces the neuronal hyperexcitability and pain hypersensitivity in bone metastasis model rats. Therefore, the enhancement of HDAC2-mediated transcriptional repression of *kcnq2* and *kcnq3* genes in DRG neurons, induced by the activation of EREG/EGFR-ERK-Runx1 signaling, likely underlies the neuronal hyperexcitability of nociceptive DRG neurons and the pain hypersensitivity in tumor-bearing rats.

Discussion

It has been documented that HDACs can remove the acetyl residues from histones to compact the chromatin structure, and inhibit gene transcription [35, 36]. Class I HDACs, in particular HDAC2 is found highly correlated to the pathology of persistent pain [37–41]. Up-regulation of HDAC2 expression is found in the lumbar spinal cord of bone cancer pain (BCP) model rats, and the enhanced HDAC2 in the spinal cord contributes to the mechanical hyperalgesia of BCP model rats by down-regulating the potassium-chloride cotransporter (KCC2) expression [11]. In line with these findings, we indeed found an increased expression of HDAC2 (but not HDAC1 and HDAC3) in ipsilateral L4/5 DRG neurons of BCP model rats. Also, the increased HDAC2 was enriched in *kcnq2* and *kcnq3* (*kcnq2/kcnq3*) genes promoter and caused histone deacetylation modification of the genes in DRG neurons of BCP model rats. Moreover, either inhibiting the activity of HDACs or knockdown HDAC2 in DRG neurons, rescues the transcriptional repression of *kcnq2/kcnq3* genes encoding Kv7(KCNQ)/M potassium channels; reverses the decreased M-current density and the increased neuronal excitability of DRG neurons, and attenuates the pain hypersensitivity in tumor-bearing rats, validating the contribution of HDAC2 to the transcriptional repression of Kv7(KCNQ)/M potassium channels in DRG neurons and the pathology of BCP in rats. Consistently, suppression of HDAC2 by either HDACs inhibitor or HDAC2 siRNA is shown to relieve pain hypersensitivity in animal models of neuropathic pain [39, 40, 64] and bone cancer pain [11, 65], supporting the involvement of HDAC2 in pathogenesis of persistent pain through regulating target

genes transcription, such as KCC2 [11], Kv1.2 [39], or KCNQ2/KCNQ3.

HDAC2 does not bind to DNA directly and is known to form a corepressor complex with other specific proteins, such as Sin3A, to regulate gene transcription [66, 67]. The Sin3A/HDAC2 complex serves as a negative regulator of the inflammatory gene program in lipopolysaccharide-activated human macrophages [68]. In addition, MeCP2 recruits HDAC2 and Sin3A to promote the deacetylation of histone tails, which results in gene silencing [67]. MeCP2 is highly expressed in the nervous system [69] and the dynamic expression of MeCP2 in the DRG after nerve injury [70] suggests a role of MeCP2 in pain modulation through transcriptional regulation. In fact, peripheral nerve injury induces an increased MeCP2 expression in injured DRGs, results in direct and indirect modulation of pain-related genes expression in the DRG, thereby underlying the pathology of neuropathic pain [43, 71]. In this study, using DEGs' gene–gene interaction network analysis for *Hdac2*, we indeed predicted the interaction of *Hdac2* with both *Sin3A* and *MeCP2*. Moreover, we found a wide co-localization of MeCP2 with HDAC2 and KCNQ2/KCNQ3 in cultured rat DRG neurons, and observed a prominent increase of MeCP2 expression across the NF200-, CGRP-, and IB4-positive DRG neurons in BCP model rats. A significant increase in the enrichment of either MeCP2 or MeCP2/HDAC2 corepressor complex in *kcnq2/kcnq3* genes promoter of DRG neurons in MRMT-1 rats, suggests an enhanced binding of MeCP2/HDAC2 corepressor complex to the *kcnq2/kcnq3* genes promoter of DRG neurons in BCP model rats. Additionally, by using intrathecal MeCP2-shRNA to knock down MeCP2 in DRG neurons, we provided further evidence demonstrating the necessary of MeCP2 for HDAC2-mediated transcriptional repression of Kv7(KCNQ)/M channels in DRG neurons and its role in bone cancer-induced pain in rats. MeCP2 binds to DNA through a methyl binding domain and facilitates the assembly of a multiprotein repressor complex that includes Sin3A and the histone deacetylases HDAC1/HDAC2 [72–74]. The MeCP2/Sin3A/HDAC2 corepressor complex is involved in the regulation of connective tissue growth factor expression in lung fibroblasts [75]. In agreement with these findings, we observed an evident co-localization of MeCP2, Sin3A, and HDAC2 in the DRG neurons, and also, knockdown of Sin3A in DRG neurons could abrogate the binding of MeCP2/HDAC2 corepressor in *kcnq2/kcnq3* genes promoter of DRG neurons, and rescue the transcriptional repression of Kv7(KCNQ)/M potassium channels in DRG neurons and the pathology of BCP in tumor-bearing rats, supporting our understanding that the formation of MeCP2/Sin3A/HDAC2 co-repressor complex by the link of MeCP2 and HDAC2 through Sin3A, is required for the transcriptional repression of *kcnq2/kcnq3* genes in DRG neurons and the pathogenesis of BCP in tumor-bearing rats.

Moreover, EGF family ligands and receptors are implicated in cell proliferation, differentiation, division, survival, and cancer development [46, 47], of these, epiregulin (EREG) has been shown to signal through EGFR to involve in pain processing [16, 60, 61]. In this study, we indeed found an increased expression of EREG, but not other EGFR ligands such as EGF and TGF-α, at both mRNA and protein levels, in ipsilateral L4/5 DRG tissues of BCP model rats, indicating the involvement of EREG in the pathology of BCP. In line with our findings, Martin and colleagues [16] reported that EREG levels and EGFR phosphorylation in the DRGs are up-regulated in mouse models of chronic inflammatory pain and neuropathic pain, and also, activation of EGFR by EREG, but not other EGFR ligands, promotes nociception. In a separate study, Kongstorp et al. [60] showed that EREG is released from intervertebral disks and induces spontaneous activity in pain pathways. EREG may trigger the expression of other growth factors and cytokines [76, 77], which in turn activates the PI3K/Akt pathway and the MAPK cascade that may affect nociceptive activity in the primary afferent nerve fibers [78], or in the spinal dorsal horn [79, 80]. Here we found that intrathecal EREG activates the ERK-Runx1 signaling cascade, promotes the nuclear translocation of transcription factor Runx1 in the DRG neurons, and up-regulates *hdac2* gene transcription. The enhanced HDAC2 in turn mediates the transcriptional repression of *kcnq2/kcnq3* genes in DRG neurons of BCP model rats, subsequently enhances the neuronal hyperexcitability and pain hypersensitivity in tumor-bearing rats. These findings suggest that EREG may be an upstream signal molecule involved in HDAC2-mediated transcriptional repression of Kv7(KCNQ)/M potassium channels in DRG neurons of BCP model rats, via the activation of ERK-Runx1 signaling pathway.

Previous findings suggest that EREG induces intracellular signaling mainly through EGFR or HER4 [62], and activation of EGFR by EREG enhances pain sensitivity [16, 60]. In this study, we found an obvious co-localization of EGFR with HDAC2 and KCNQ2/KCNQ3 in cultured rat DRG neurons, and observed an increased expression of EGFR in ipsilateral L4/5 DRG tissues of BCP model rats, raising the possibility for the involvement of EGFR in the pathogenesis of BCP. In fact, EGFR inhibition rescues the transcriptional repression of Kv7(KCNQ)/M channels in DRG neurons and the pain hypersensitivity in BCP model rats, supporting our understanding that the upregulated EGFR in DRG neurons probably involves in the transcriptional repression of *kcnq2/kcnq3* genes and the pathogenesis of BCP in bone metastasis model rats.

Consistently, several studies have shown that EGFR is involved in pain processing [16, 60, 61], and EGFR inhibition is the first-line treatment for non-small cell lung cancer [61, 81], and also, the EGFR inhibition provides rapid relief of cancer pain [50, 63, 82, 83]. Furthermore, data from EGFR knockdown also support the involvement of EGFR in EREG-induced activation of ERK-Runx1 signaling and the upregulated HDAC2, and also, in HDAC2-mediated *kcnq2/kcnq3* genes transcriptional repression in DRG neurons and in EREG-induced pain hypersensitivity in naïve rats. In addition, knockdown of EGFR effectively restores the activation of ERK-Runx1 signaling and HDAC2-mediated transcriptional repression of *kcnq2/kcnq3* genes in DRG neurons of BCP model rats, subsequently reduces the neuronal hyperexcitability and pain hypersensitivity in tumor-bearing rats, supporting the roles of EGFR in HDAC2-mediated transcriptional repression of Kv7(KCNQ)/M potassium channels and the pathogenesis of BCP in tumor-bearing rats.

The downstream effects of EGFR are mediated by a number of signaling pathways including the RAS/ERK cascade [17, 51–53], which regulates multiple pain responses [54–57]. The activation of ERK signaling is implicated in post-translational modifications, especially the phosphorylated modification of Runx1 [18, 19], which is required for the differentiation of nociceptors and the pathogenesis of persistent pain [20, 21, 58, 59]. Also, Runx1 has been shown to transcriptionally regulate HDAC2 expression in breast cancer tissues [22]. Our present data also revealed that disrupting the activation of ERK-Runx1 signaling in DRG neurons, either by ERK inhibitor or Runx1 siRNA, abrogates HDAC2-mediated transcriptional repression of *kcnq2/kcnq3* genes, and reduces the neuronal hyperexcitability and pain hypersensitivity in bone metastasis model rats. These findings suggest that the enhancement of HDAC2-mediated transcriptional repression of *kcnq2/kcnq3* genes in DRG neurons, induced by the activation of EREG/EGFR-ERK-Runx1 signaling, likely underlies the neuronal hyperexcitability of nociceptive DRG neurons and the pain hypersensitivity in tumor-bearing rats (Fig. 8).

Limitations of the study. First, in consideration of other HDACs in particular class I HDACs (HDAC1, 3, 8) and class II HDACs (HDAC4, 5, 7, 9 in class IIa and HDAC6, 10 in class IIb), the role of HDAC1 [84–87] and HDAC3 [88, 89] in neuropathic pain development has been reported in several studies. In parallel, HDAC1 is found contributing to the pathology of BCP in animal models [10, 90, 91]. HDAC8 is involved in important cellular processes such as cell cycle, migration, and differentiation, and implicates in cancer progression [92, 93]. Nevertheless, the role of HDAC8 in pain processing is

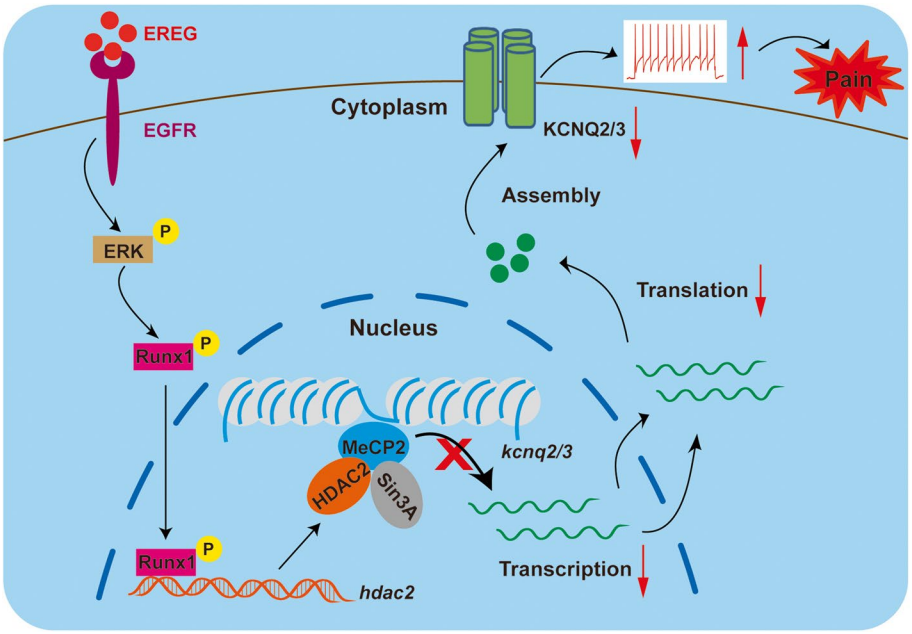

Fig. 8 Schematic summary of HDAC2-mediated *kcnq2/kcnq3* genes transcription repression in bone cancer pain. The HDAC2-mediated transcriptional repression of kcnq2 and kcnq3 genes, induced by the activation of EREG/EGFR-ERK-Runx1 signaling, contributes to the sensitization of DRG neurons and the pathogenesis of BCP in rats. Note that HDAC2 needs to form corepressor complex with MeCP2 and Sin3A, and EREG is an upstream signal molecule for HDAC2-mediated gene transcription repression. EREG/EGFR-ERK-Runx1 signaling underlies the HDAC2-mediated gene transcription repression

poorly reported. Contribution of class IIa HDAC members (HDAC4, 5, 7, 9) to chronic pain development has been documented in various inflammatory and neuropathic pain models [94–98]. HDAC6, a class IIb HDACs member also plays important role in the pathogenesis of inflammatory pain [99, 100], neuropathic pain [101, 102], and bone cancer pain [103], whereas HDAC10, another class IIb HDACs member is not found involving in pain processing. Although these HDAC members play important role in the development of chronic pain including BCP, there is, however, no experimental evidence demonstrating the transcriptional regulation of *kcnq2/kcnq3* genes by them to our knowledge. We suppose that for these HDAC members, there are probably distinct mechanisms underlying the regulatory role in the pathology of BCP. In fact, HDACs are correlated with the downregulation of μ-opioid receptor in the DRG during the pathogenesis of BCP [90]. Activation of glial cells and the glia-mediated neuroinflammation in the DRG and spinal dorsal horn may serve as a potential mechanism underlying the contribution of HDAC1 to BCP development [10, 91]. HDAC6 contributes to the pathology of BCP through the activation of spinal NOD-like receptor pyrin domain containing 3 (NLRP3) inflammasome [103]. Given the functional redundancy and potential compensatory mechanisms within the HDAC family, investigating these HDAC members will provide a more comprehensive understanding of the regulatory networks involved in the pathogenesis of BCP.

Second, the diversity of DRG sensory neurons is an important physiological and pathological feature allowing the discrimination between various types of sensations [104]. For instance, small- and medium-diameter neurons with unmyelinated C-fibers or lightly myelinated Aδ-fibers, including peptidergic or non-peptidergic neurons, are responsible for nociception (i.e. pain perception), thermoception, pruriception (i.e. itch perception) and gentle touch (C-fiber low-threshold mechanoreceptors). Whereas large-diameter neurons with myelinated Aα- and Aβ-fibers conduct proprioception and mechanoreception (non-painful tactile, e.g. touch) [104, 105]. Our findings revealed that changes in HDAC2, MeCP2, EGFR, etc. are presented in almost all types of neurons in the DRG, thus the M current that result from changes in the above signals in non-nociceptive neurons will lead to relevant changes in their excitability. These alterations in non-nociceptive DRG neurons, therefore, will exert influence on their behavior on other sensory models such as touch and itch. Contribution of altered HDAC2, MeCP2, EGFR, and KCNQ in the DRG neurons to other sensory models e.g. itch need be further studied.

Third, EGFR, a member of the membrane-bound receptor tyrosine kinases (RTKs), can be shuttled into the cell nucleus upon ligand binding and other stimuli [106], where the nuclear EGFR acts as a transcriptional regulator, transmits signals, and is involved in multiple biological functions, including cell proliferation, tumorigenesis and tumor progression [107]. Recent studies have shown that endocytosis and endosomal sorting are involved in the nuclear transport of cell surface RTKs [108], in which both clathrin-dependent [109] and clathrin-independent [110] endocytosis are involved in the nuclear translocation of EGFR family RTKs. In addition, many membrane-surface RTKs, including EGFR family receptors, translocate to the nucleus by importin β-dependent mechanisms [111], and there, the nuclear transport of the EGFR is regulated by coat protein complex I (COPI)-mediated vesicular trafficking from the Golgi to the endoplasmic reticulum (ER), and then transport to the nucleus by the Sec61 translocon [112, 113]. In line with these notions, we indeed found that some EGFR is expressed in the nucleus in addition to their usual plasma membrane localization, as observed mainly expressing in the cytoplasm of DRG neurons. The exact shuttling mechanism of EGFR in and out of the nucleus is unclear. A better understanding of the molecular mechanism of EGFR trafficking will shed light on the potential therapeutic targets of anti-EGFR therapies for clinical application.

Last, the pathophysiological mechanism of BCP is complex and multifactorial, involving various interactions between tumor cells, bone cells, activated inflammatory cells, and bone-innervating neurons [114]. It includes inflammatory and neuropathic processes, which are modified at the levels of peripheral nociceptors and central nervous system, e.g. abnormal activities in primary sensory neurons have been implicated in the process of BCP [115, 116]. In addition, tumor-derived factors have been shown to sensitize and injure primary sensory neurons [117]. A better understanding of the peripheral nociceptors is essential for the successful treatment of bone cancer pain. Clinically, multimodal approaches such as surgical intervention, radiotherapy, and pharmacotherapy are recommended to manage BCP [114]. In view of pharmacotherapy, opioids, nonsteroidal anti-inflammatory drugs (NSAIDs), and antidepressants are among the first-line therapies, but their efficacy is limited or their use can be restricted due to serious side effects [118]. The World Health Organization (WHO) has proposed a BCP treatment strategy based on a three-step analgesic ladder starting from non-opioids to weak opioids to strong opioids [119]. In addition, additional adjuvant therapies, including bone-targeted therapies (anti-nerve growth factor antibodies; receptor activator of nuclear factor kappa-B ligand (RANKL) inhibitors; osteoclast inhibitors, such as bisphosphonates

and denosumab) and adjuvants (corticosteroids, anticonvulsants) are used to alleviate BCP in some patients, however, each of these treatment options is accompanied by limitations in their use [114].

Considerable progress has been made in recent years regarding the role of primary sensory neurons in nociceptive processing, leading to the development of new therapeutic approaches that target nociceptors [116]. Some of these therapies are currently in clinical use [120] or will be available soon [121, 122]. Recently, there has been an increasing interest in the role of ion channels and receptors in chronic pain, including BCP [123]. Understanding the mechanisms underlying ion channel dysregulation in BCP is important for the development of new therapies for BCP. For instance, targeting transient receptor potential (TRP) channels, acid-sensing ion channels (ASICs), voltage-gated sodium channels and potassium channels, as well as Piezo channels and P2X receptors have been considered a new strategic approach for achieving analgesia in BCP [123, 124]. In this study, we demonstrated that the transcriptional repression of *kcnq2/kcnq3* genes in DRG neurons plays important role in the pathogenesis of BCP, suggesting that targeting Kv7(KCNQ)/M potassium channels may be a novel therapeutic strategy for BCP [2].

Besides, epigenetic modifications and neurotrophins-mediated tumor neurogenesis have been shown to be involved in the formation of chronic pain and pain relief [125, 126]. Intrathecal administration of clinically available pan-HDAC inhibitor such as trichostatin A (TSA) or suberoylanilide hydroxamic acid (SAHA) alleviates tactile hypersensitivity and enhances the analgesic effect of morphine in BCP model rats [10, 11, 65]. Recently, EGFR and its natural ligand epiregulin (EREG) have received attention for the therapeutic potential against pathological pain [16, 17, 50]. EGFR belongs to the well-studied ErbB family of receptor tyrosine kinases (RTKs) that have key roles in the development and progression of many cancers [127]. Anti-EGFR therapy using small-molecule EGFR tyrosine kinase inhibitors (TKIs) or anti-EGFR monocloncal antibody (mAb) has become one of the leading therapeutic strategies to combat several malignancies in patients [128, 129], and these clinically available EGFR kinase inhibitors and mAb also provide rapid relief of cancer pain [130, 131]. It is shown that EREG, but not other EGFR ligands (EGF, amphiregulin, betacellulin, TGF-α), enhances formalin-induced nocifensive behaviors in mice with EREG administration alone being sufficient to induce heat and mechanical hypersensitivity [16]. EREG may have roles in inflammation-driven pain, and inhibition of EREG reverses hypersensitivity in animal models of chronic pain [132]. Understanding the notion that EREG is the primary endogenous activator of EGFR-related pain hypersensitivity, directly targeting EREG may be an effective treatment strategy for BCP management [50]. Together with our findings showing the involvement of EREG/EGFR-ERK-Runx1 signaling in HDAC2-mediated transcriptional repression of *kcnq2/kcnq3* genes in DRG neurons of BCP model rats, we suggest that targeted therapy with EGFR kinase inhibitors, HDAC inhibitors, Kv7(KCNQ)/M potassium channels openers, or combined with multitarget approach targeting these signaling pathway sites, can be designed as potential therapeutic strategies for the treatment of BCP in clinic. Our present findings will 'filling in the gaps' of the current understanding for the pathological mechanisms and the clinical therapeutic strategies of BCP.

In conclusion, this study demonstrates that the HDAC2-mediated transcriptional repression of *kcnq2/kcnq3* genes in DRG neurons, via the activation of EREG/EGFR-ERK-Runx1 signaling, contributes to the sensitization of DRG neurons and the pathogenesis of bone cancer pain in rats. Our findings identify a potentially targetable mechanism that may cause bone metastasis-associated pain in cancer patients.

Supplementary Information

The online version contains supplementary material available at https://doi.org/10.1186/s12964-024-01797-2.

Supplementary Material 1: Figs. S1 to S15. Tables S1 to S4.

Acknowledgements
The authors thank Novartis Oncology Research, Basel for gifting MRMT-1 rat mammary gland carcinoma cells.

Authors' contributions
G.G.X. conceived and designed research. Z.X.Z, Y.T., S.L., and H.B.J. performed experiments. Y.T. provided assistant and analyzed the data. J.C. provided technical support for experiments. M.L. participated in the results discussion and some experiments design. G.G.X. and Z.X.Z. drafted the manuscript. All authors commented on and approved the final draft.

Funding
This work was supported by the grants from National Natural Science Foundation of China (82371227, 82171226, 81974169, 81671085), Natural Science Foundation of Beijing Municipality (7222105), National Key Research and Development Program of China (2019YFC1712104), and King's College London (KCL)-Peking University Health Science Center (PKUHSC) Joint Institute for Medical Research (JI) Program (BMU2021KCL001).

Availability of data and materials
All the data generated during the current study are available from the corresponding author upon reasonable request.

Data availability
No datasets were generated or analysed during the current study.

Declarations

Ethics approval and consent to participate
All experiments were approved by the Animal Care and Use Committee of Peking University (Approval number: BCJB0019) and performed in accordance with both the National Institutes of Health Guide for the Care and Use

of Laboratory Animals and the ARRIVE (Animal Research: Reporting of In Vivo Experiments) guidelines.

Competing interests
The authors declare no competing interests.

Received: 12 June 2024 Accepted: 18 August 2024
Published online: 27 August 2024

References

1. Zheng Q, Fang D, Cai J, Wan Y, Han JS, Xing GG. Enhanced excitability of small dorsal root ganglion neurons in rats with bone cancer pain. Mol Pain. 2012;8:24.
2. Zheng Q, Fang D, Liu M, Cai J, Wan Y, Han JS, Xing GG. Suppression of KCNQ/M (Kv7) potassium channels in dorsal root ganglion neurons contributes to the development of bone cancer pain in a rat model. Pain. 2013;154:434–48.
3. Jones F, Gamper N, Gao H. Kv7 channels and excitability disorders. Handb Exp Pharmacol. 2021;267:185–230.
4. Wang HS, Pan Z, Shi W, Brown BS, Wymore RS, Cohen IS, Dixon JE, McKinnon D. KCNQ2 and KCNQ3 potassium channel subunits: molecular correlates of the M-channel. Science. 1998;282:1890–3.
5. Soldovieri MV, Miceli F, Taglialatela M. Driving with no brakes: molecular pathophysiology of Kv7 potassium channels. Physiology (Bethesda). 2011;26:365–76.
6. Baculis BC, Zhang J, Chung HJ. The role of K(v)7 channels in neural plasticity and behavior. Front Physiol. 2020;11:568667.
7. Brown DA, Passmore GM. Neural KCNQ (Kv7) channels. Br J Pharmacol. 2009;156:1185–95.
8. Bannister AJ, Kouzarides T. Regulation of chromatin by histone modifications. Cell Res. 2011;21:381–95.
9. Kuo MH, Allis CD. Roles of histone acetyltransferases and deacetylases in gene regulation. BioEssays. 1998;20:615–26.
10. He XT, Hu XF, Zhu C, Zhou KX, Zhao WJ, Zhang C, Han X, Wu CL, Wei YY, Wang W, et al. Suppression of histone deacetylases by SAHA relieves bone cancer pain in rats via inhibiting activation of glial cells in spinal dorsal horn and dorsal root ganglia. J Neuroinflammation. 2020;17:125.
11. Hou X, Weng Y, Wang T, Ouyang B, Li Y, Song Z, Pan Y, Zhang Z, Zou W, Huang C, Guo Q. Suppression of HDAC2 in spinal cord alleviates mechanical hyperalgesia and restores KCC2 expression in a rat model of bone cancer pain. Neuroscience. 2018;377:138–49.
12. Banks CAS, Zhang Y, Miah S, Hao Y, Adams MK, Wen Z, Thornton JL, Florens L, Washburn MP. Integrative modeling of a Sin3/HDAC complex sub-structure. Cell Rep. 2020;31:107516.
13. Clem BF, Clark BJ. Association of the mSin3A-histone deacetylase 1/2 corepressor complex with the mouse steroidogenic acute regulatory protein gene. Mol Endocrinol. 2006;20:100–13.
14. Mahgoub M, Adachi M, Suzuki K, Liu X, Kavalali ET, Chahrour MH, Monteggia LM. MeCP2 and histone deacetylases 1 and 2 in dorsal striatum collectively suppress repetitive behaviors. Nat Neurosci. 2016;19:1506–12.
15. Piazza R, Magistroni V, Mogavero A, Andreoni F, Ambrogio C, Chiarle R, Mologni L, Bachmann PS, Lock RB, Collini P, et al. Epigenetic silencing of the proapoptotic gene BIM in anaplastic large cell lymphoma through an MeCP2/SIN3a deacetylating complex. Neoplasia. 2013;15:511–22.
16. Martin LJ, Smith SB, Khoutorsky A, Magnussen CA, Samoshkin A, Sorge RE, Cho C, Yosefpour N, Sivaselvachandran S, Tohyama S, et al. Epiregulin and EGFR interactions are involved in pain processing. J Clin Invest. 2017;127:3353–66.
17. Binshtok U, Sprinzak D. The domino effect in EGFR-ERK signaling. Dev Cell. 2018;46:128–30.
18. Santoni G, Nabissi M, Amantini C, Santoni M, Ricci-Vitiani L, Pallini R, Maggi F, Morelli MB. ERK phosphorylation regulates the Aml1/Runx1 splice variants and the TRP channels expression during the differentiation of glioma stem cell lines. Cells. 2021;10:2052.
19. Friedman AD. Cell cycle and developmental control of hematopoiesis by Runx1. J Cell Physiol. 2009;219:520–4.
20. Chen CL, Broom DC, Liu Y, de Nooij JC, Li Z, Cen C, Samad OA, Jessell TM, Woolf CJ, Ma Q. Runx1 determines nociceptive sensory neuron phenotype and is required for thermal and neuropathic pain. Neuron. 2006;49:365–77.
21. Yuan ZL, Liu XD, Zhang ZX, Li S, Tian Y, Xi K, Cai J, Yang XM, Liu M, Xing GG. Activation of GDNF-ERK-Runx1 signaling contributes to P2X3R gene transcription and bone cancer pain. iScience. 2022;25:104936.
22. Zhang Z, Qiu N, Yin J, Zhang J, Liu H, Guo W, Liu M, Liu T, Chen D, Luo K, et al. SRGN crosstalks with YAP to maintain chemoresistance and stemness in breast cancer cells by modulating HDAC2 expression. Theranostics. 2020;10:4290–307.
23. Yang Y, Li S, Jin ZR, Jing HB, Zhao HY, Liu BH, Liang YJ, Liu LY, Cai J, Wan Y, Xing GG. Decreased abundance of TRESK two-pore domain potassium channels in sensory neurons underlies the pain associated with bone metastasis. Sci Signal. 2018;11:eaao5150.
24. Li G, Ma F, Gu Y, Huang LY. Analgesic tolerance of opioid agonists in mutant mu-opioid receptors expressed in sensory neurons following intrathecal plasmid gene delivery. Mol Pain. 2013;9:63.
25. Towne C, Pertin M, Beggah AT, Aebischer P, Decosterd I. Recombinant adeno-associated virus serotype 6 (rAAV2/6)-mediated gene transfer to nociceptive neurons through different routes of delivery. Mol Pain. 2009;5:52.
26. Gendron L, Lucido AL, Mennicken F, O'Donnell D, Vincent JP, Stroh T, Beaudet A. Morphine and pain-related stimuli enhance cell surface availability of somatic delta-opioid receptors in rat dorsal root ganglia. J Neurosci. 2006;26:953–62.
27. Wu WP, Xu XJ, Hao JX. Chronic lumbar catheterization of the spinal subarachnoid space in mice. J Neurosci Methods. 2004;133:65–9.
28. Jasmin L, Ohara PT. Long-term intrathecal catheterization in the rat. J Neurosci Methods. 2001;110:81–9.
29. Jiang H, Liu JP, Xi K, Liu LY, Kong LY, Cai J, Cai SQ, Han XY, Song JG, Yang XM, et al. Contribution of AMPA receptor-mediated LTD in LA/BLA-CeA pathway to comorbid aversive and depressive symptoms in neuropathic pain. J Neurosci. 2021;41:7278–99.
30. Chaplan SR, Bach FW, Pogrel JW, Chung JM, Yaksh TL. Quantitative assessment of tactile allodynia in the rat paw. J Neurosci Methods. 1994;53:55–63.
31 Hargreaves K, Dubner R, Brown F, Flores C, Joris J. A new and sensitive method for measuring thermal nociception in cutaneous hyperalgesia. Pain. 1988;32:77–88.
32. Rivlin AS, Tator CH. Objective clinical assessment of motor function after experimental spinal cord injury in the rat. J Neurosurg. 1977;47:577–81.
33. Najar M, Alsabri SG, Guedi GG, Merimi M, Lavoie F, Grabs D, Pelletier JP, Martel-Pelletier J, Benderdour M, Fahmi H. Role of epigenetics and the transcription factor Sp1 in the expression of the D prostanoid receptor 1 in human cartilage. Front Cell Dev Biol. 2023;11:1256998.
34. Gao Y, Bai L, Zhou W, Yang Y, Zhang J, Li L, Jiang M, Mi Y, Li TT, Zhang X, et al. PARP-1-regulated TNF-α expression in the dorsal root ganglia and spinal dorsal horn contributes to the pathogenesis of neuropathic pain in rats. Brain Behav Immun. 2020;88:482–96.
35. Seto E, Yoshida M. Erasers of histone acetylation: the histone deacetylase enzymes. Cold Spring Harb Perspect Biol. 2014;6:a018713.
36. Ning L, Rui X, Bo W, Qing G. The critical roles of histone deacetylase 3 in the pathogenesis of solid organ injury. Cell Death Dis. 2021;12:734.
37. Zhang J, Chen SR, Zhou MH, Jin D, Chen H, Wang L, DePinho RA, Pan HL. HDAC2 in primary sensory neurons constitutively restrains chronic pain by repressing α2δ-1 expression and associated NMDA receptor activity. J Neurosci. 2022;42:8918–35.
38. Miao J, Chen Z, Wu Y, Hu Q, Ji T. Sp1 inhibits PGC-1α via HDAC2-catalyzed histone deacetylation in chronic constriction injury-induced neuropathic pain. ACS Chem Neurosci. 2022;13:3438–52.
39 Li Z, Guo Y, Ren X, Rong L, Huang M, Cao J, Zang W. HDAC2, but not HDAC1, regulates Kv1.2 expression to mediate neuropathic pain in CCI rats. Neuroscience. 2019;408:339–48.
40. Wang XM, Gu P, Saligan L, Iadarola M, Wong SSC, Ti LK, Cheung CW. Dysregulation of EAAT2 and VGLUT2 spinal glutamate transports via histone deacetylase 2 (HDAC2) contributes to paclitaxel-induced painful neuropathy. Mol Cancer Ther. 2020;19:2196–209.
41. Miao J, Zhou X, Ji T, Chen G. NF-κB p65-dependent transcriptional regulation of histone deacetylase 2 contributes to the chronic constriction

injury-induced neuropathic pain via the microRNA-183/TXNIP/NLRP3 axis. J Neuroinflammation. 2020;17:225.
42. Kelly RD, Cowley SM. The physiological roles of histone deacetylase (HDAC) 1 and 2: complex co-stars with multiple leading parts. Biochem Soc Trans. 2013;41:741–9.
43. Sun N, Yu L, Gao Y, Ma L, Ren J, Liu Y, Gao DS, Xie C, Wu Y, Wang L, et al. MeCP2 epigenetic silencing of Oprm1 gene in primary sensory neurons under neuropathic pain conditions. Front Neurosci. 2021;15:743207.
44. Adams GE, Chandru A, Cowley SM. Co-repressor, co-activator and general transcription factor: the many faces of the Sin3 histone deacetylase (HDAC) complex. Biochem J. 2018;475:3921–32.
45. Kadamb R, Mittal S, Bansal N, Batra H, Saluja D. Sin3: insight into its transcription regulatory functions. Eur J Cell Biol. 2013;92:237–46.
46. Esparís-Ogando A, Montero JC, Arribas J, Ocaña A, Pandiella A. Targeting the EGF/HER ligand-receptor system in cancer. Curr Pharm Des. 2016;22:5887–98.
47. Burgess AW. Regulation of signaling from the epidermal growth factor family. J Phys Chem B. 2022;126:7475–85.
48. Abud HE, Chan WH, Jardé T. Source and impact of the EGF family of ligands on intestinal stem cells. Front Cell Dev Biol. 2021;9:685665.
49. Wang Z. ErbB receptors and cancer. Methods Mol Biol. 2017;1652:3–35.
50. Borges JP, Mekhail K, Fairn GD, Antonescu CN, Steinberg BE. Modulation of pathological pain by epidermal growth factor receptor. Front Pharmacol. 2021;12:642820.
51. Bader M, Yang Y, Sun Y, Hu R, Yan J, Wang Z, Li W, Jiang H. Morphine promotes microglial activation by upregulating the EGFR/ERK signaling pathway. Plos One. 2021;16:e0256870.
52. Zhao Y, Ma J, Fan Y, Wang Z, Tian R, Ji W, Zhang F, Niu R. TGF-beta transactivates EGFR and facilitates breast cancer migration and invasion through canonical Smad3 and ERK/Sp1 signaling pathways. Mol Oncol. 2018;12:305–21.
53. Sooro MA, Zhang N, Zhang P. Targeting EGFR-mediated autophagy as a potential strategy for cancer therapy. Int J Cancer. 2018;143:2116–25.
54. Kondo M, Shibuta I. Extracellular signal-regulated kinases (ERK) 1 and 2 as a key molecule in pain research. J Oral Sci. 2020;62:147–9.
55. Wang B, Liu S, Fan B, Xu X, Chen Y, Lu R, Xu Z, Liu X. PKM2 is involved in neuropathic pain by regulating ERK and STAT3 activation in rat spinal cord. J Headache Pain. 2018;19:7.
56. Zhang J, Li Z, Chen F, Liu H, Wang H, Li X, Liu X, Wang J, Zheng Z. TGF-beta1 suppresses CCL3/4 expression through the ERK signaling pathway and inhibits intervertebral disc degeneration and inflammation-related pain in a rat model. Exp Mol Med. 2017;49:e379.
57. Ma W, Quirion R. The ERK/MAPK pathway, as a target for the treatment of neuropathic pain. Expert Opin Ther Targets. 2005;9:699–713.
58. Li Y, Guo X, Sun L, Xiao J, Su S, Du S, Li Z, Wu S, Liu W, Mo K, et al. N(6)-Methyladenosine demethylase FTO contributes to neuropathic pain by stabilizing G9a expression in primary sensory neurons. Adv Sci (Weinh). 2020;7:1902402.
59. Ugarte GD, Diaz E, Biscaia M, Stehberg J, Montecino M, van Zundert B. Transcription of the pain-related TRPV1 gene requires Runx1 and C/EBPbeta factors. J Cell Physiol. 2013;228:860–70.
60. Kongstorp M, Schjølberg T, Jacobsen DP, Haugen F, Gjerstad J. Epiregulin is released from intervertebral disks and induces spontaneous activity in pain pathways. Pain Rep. 2019;4:e718.
61. Gazdar AF. Epidermal growth factor receptor inhibition in lung cancer: the evolving role of individualized therapy. Cancer Metastasis Rev. 2010;29:37–48.
62. Komurasaki T, Toyoda H, Uchida D, Morimoto S. Epiregulin binds to epidermal growth factor receptor and ErbB-4 and induces tyrosine phosphorylation of epidermal growth factor receptor, ErbB-2, ErbB-3 and ErbB-4. Oncogene. 1997;15:2841–8.
63. Kersten C, Cameron MG, Laird B, Mjåland S. Epidermal growth factor receptor-inhibition (EGFR-I) in the treatment of neuropathic pain. Br J Anaesth. 2015;115:761–7.
64. Pryce KD, Serafini RA, Ramakrishnan A, Nicolais A, Giosan IM, Polizu C, Torres-Berrío A, Vuppala S, Kronman H, Ruiz A, et al. Oxycodone withdrawal induces HDAC1/HDAC2-dependent transcriptional maladaptations in the reward pathway in a mouse model of peripheral nerve injury. Nat Neurosci. 2023;26:1229–44.
65. Hou X, Weng Y, Ouyang B, Ding Z, Song Z, Zou W, Huang C, Guo Q. HDAC inhibitor TSA ameliorates mechanical hypersensitivity and potentiates analgesic effect of morphine in a rat model of bone cancer pain by restoring μ-opioid receptor in spinal cord. Brain Res. 2017;1669:97–105.
66. Saunders A, Huang X, Fidalgo M, Reimer MH Jr, Faiola F, Ding J, Sánchez-Priego C, Guallar D, Sáenz C, Li D, Wang J. The SIN3A/HDAC corepressor complex functionally cooperates with NANOG to promote pluripotency. Cell Rep. 2017;18:1713–26.
67. Kavalali ET, Nelson ED, Monteggia LM. Role of MeCP2, DNA methylation, and HDACs in regulating synapse function. J Neurodev Disord. 2011;3:250–6.
68. John SP, Sun J, Carlson RJ, Cao B, Bradfield CJ, Song J, Smelkinson M, Fraser IDC. IFIT1 exerts opposing regulatory effects on the inflammatory and interferon gene programs in LPS-activated human macrophages. Cell Rep. 2018;25:95-106.e106.
69. Skene PJ, Illingworth RS, Webb S, Kerr AR, James KD, Turner DJ, Andrews R, Bird AP. Neuronal MeCP2 is expressed at near histone-octamer levels and globally alters the chromatin state. Mol Cell. 2010;37:457–68.
70. Manners MT, Tian Y, Zhou Z, Ajit SK. MicroRNAs downregulated in neuropathic pain regulate MeCP2 and BDNF related to pain sensitivity. FEBS Open Bio. 2015;5:733–40.
71. Manners MT, Ertel A, Tian Y, Ajit SK. Genome-wide redistribution of MeCP2 in dorsal root ganglia after peripheral nerve injury. Epigenetics Chromatin. 2016;9:23.
72. Jones PL, Veenstra GJ, Wade PA, Vermaak D, Kass SU, Landsberger N, Strouboulis J, Wolffe AP. Methylated DNA and MeCP2 recruit histone deacetylase to repress transcription. Nat Genet. 1998;19:187–91.
73. Nan X, Ng HH, Johnson CA, Laherty CD, Turner BM, Eisenman RN, Bird A. Transcriptional repression by the methyl-CpG-binding protein MeCP2 involves a histone deacetylase complex. Nature. 1998;393:386–9.
74. Razin A. CpG methylation, chromatin structure and gene silencing-a three-way connection. Embo j. 1998;17:4905–8.
75. Hua HS, Wen HC, Lee HS, Weng CM, Yuliani FS, Kuo HP, Chen BC, Lin CH. Endothelin-1 induces connective tissue growth factor expression in human lung fibroblasts by disrupting HDAC2/Sin3A/MeCP2 corepressor complex. J Biomed Sci. 2023;30:40.
76. Harada M, Kamimura D, Arima Y, Kohsaka H, Nakatsuji Y, Nishida M, Atsumi T, Meng J, Bando H, Singh R, et al. Temporal expression of growth factors triggered by epiregulin regulates inflammation development. J Immunol. 2015;194:1039–46.
77. Murakami M, Harada M, Kamimura D, Ogura H, Okuyama Y, Kumai N, Okuyama A, Singh R, Jiang JJ, Atsumi T, et al. Disease-association analysis of an inflammation-related feedback loop. Cell Rep. 2013;3:946–59.
78. Fang D, Kong LY, Cai J, Li S, Liu XD, Han JS, Xing GG. Interleukin-6-mediated functional upregulation of TRPV1 receptors in dorsal root ganglion neurons through the activation of JAK/PI3K signaling pathway: roles in the development of bone cancer pain in a rat model. Pain. 2015;156:1124–44.
79. Pezet S, Marchand F, D'Mello R, Grist J, Clark AK, Malcangio M, Dickenson AH, Williams RJ, McMahon SB. Phosphatidylinositol 3-kinase is a key mediator of central sensitization in painful inflammatory conditions. J Neurosci. 2008;28:4261–70.
80. Song XS, Cao JL, Xu YB, He JH, Zhang LC, Zeng YM. Activation of ERK/CREB pathway in spinal cord contributes to chronic constrictive injury-induced neuropathic pain in rats. Acta Pharmacol Sin. 2005;26:789–98.
81. Sun X, Xu S, Yang Z, Zheng P, Zhu W. Epidermal growth factor receptor (EGFR) tyrosine kinase inhibitors for the treatment of non-small cell lung cancer: a patent review (2014-present). Expert Opin Ther Pat. 2021;31:223–38.
82. Scheff NN, Ye Y, Conley ZR, Quan JW, Lam YVR, Klares R 3rd, Singh K, Schmidt BL, Aouizerat BE. A disintegrin and metalloproteinase domain 17-epidermal growth factor receptor signaling contributes to oral cancer pain. Pain. 2020;161:2330–43.
83. Cameron MG, Kersten C. Prospective case series of neuropathic cancer pain in patients treated with an EGFR-inhibitor. Palliat Med. 2022;36:1154–62.
84. Borgonetti V, Mugnaini C, Corelli F, Galeotti N. The selective CB2 agonist COR167 reduced symptoms in a mice model of trauma-induced peripheral neuropathy through HDAC-1 inhibition. Biomedicines. 2023;11:1546.
85. Zheng HL, Sun SY, Jin T, Zhang M, Zeng Y, Liu Q, Yang K, Wei R, Pan Z, Lin F. Transcription factor ETS proto-oncogene 1 contributes to

neuropathic pain by regulating histone deacetylase 1 in primary afferent neurons. Mol Pain. 2023;19:17448069231152124.
86. Xie Y, Li Z, Xu H, Ma J, Li T, Shi C, Jin J. Downregulation of Sp1 inhibits the expression of HDAC1/SOX10 to alleviate neuropathic pain-like behaviors after spinal nerve ligation in mice. ACS Chem Neurosci. 2022;13:1446–55.
87. Sanna MD, Galeotti N. The HDAC1/c-JUN complex is essential in the promotion of nerve injury-induced neuropathic pain through JNK signaling. Eur J Pharmacol. 2018;825:99–106.
88. Wei W, Liu Y, Qiu Y, Chen M, Wang Y, Han Z, Chai Y, Sase A. Characterization of acetylation of histone H3 at lysine 9 in the trigeminal ganglion of a rat trigeminal neuralgia model. Oxid Med Cell Longev. 2022;2022:1–13.
89. Guo A, Li J, Luo L, Chen C, Lu Q, Ke J, Feng X. Valproic acid mitigates spinal nerve ligation-induced neuropathic pain in rats by modulating microglial function and inhibiting neuroinflammatory response. Int Immunopharmacol. 2021;92:107332.
90. He XT, Zhou KX, Zhao WJ, Zhang C, Deng JP, Chen FM, Gu ZX, Li YQ, Dong YL. Inhibition of histone deacetylases attenuates morphine tolerance and restores MOR expression in the DRG of BCP rats. Front Pharmacol. 2018;9:509.
91. Hu XF, He XT, Zhou KX, Zhang C, Zhao WJ, Zhang T, Li JL, Deng JP, Dong YL. The analgesic effects of triptolide in the bone cancer pain rats via inhibiting the upregulation of HDACs in spinal glial cells. J Neuroinflammation. 2017;14:213.
92. Chakrabarti A, Oehme I, Witt O, Oliveira G, Sippl W, Romier C, Pierce RJ, Jung M. HDAC8: a multifaceted target for therapeutic interventions. Trends Pharmacol Sci. 2015;36:481–92.
93 Kim JY, Cho H, Yoo J, Kim GW, Jeon YH, Lee SW, Kwon SH. Pathological role of HDAC8: cancer and beyond. Cells. 2022;11:3161.
94. Bai G, Wei D, Zou S, Ren K, Dubner R. Inhibition of class II histone deacetylases in the spinal cord attenuates inflammatory hyperalgesia. Mol Pain. 2010;6:51.
95. Zhao B, Fu J, Ni H, Xu L, Xu C, He Q, Ni C, Wang Y, Kuang J, Tang M, et al. Catalpol ameliorates CFA-induced inflammatory pain by targeting spinal cord and peripheral inflammation. Front Pharmacol. 2022;13:1010483.
96. Wen J, He T, Qi F, Chen H. MiR-206-3p alleviates chronic constriction injury-induced neuropathic pain through targeting HDAC4. Exp Anim. 2019;68:213–20.
97. Gu P, Pan Z, Wang XM, Sun L, Tai LW, Cheung CW. Histone deacetylase 5 (HDAC5) regulates neuropathic pain through SRY-related HMG-box 10 (SOX10)-dependent mechanism in mice. Pain. 2018;159:526–39.
98. Lei M, Lin H, Shi D, Hong P, Song H, Herman B, Liao Z, Yang C. Molecular mechanism and therapeutic potential of HDAC9 in intervertebral disc degeneration. Cell Mol Biol Lett. 2023;28:104.
99. Cheng DW, Xu Y, Chen T, Zhen SQ, Meng W, Zhu HL, Liu L, Xie M, Zhen F. Emodin inhibits HDAC6 mediated NLRP3 signaling and relieves chronic inflammatory pain in mice. Exp Ther Med. 2024;27:44.
100. Barter MJ, Butcher A, Wang H, Tsompani D, Galler M, Rumsby EL, Culley KL, Clark IM, Young DA. HDAC6 regulates NF-κB signalling to control chondrocyte IL-1-induced MMP and inflammatory gene expression. Sci Rep. 2022;12:6640.
101. Yue W, Sun N, Zhang J, Zhang W, Wu Y, Qu X, Zong J, Xu G. Alleviated diabetic osteoporosis and peripheral neuropathic pain by Rehmannia glutinosa Libosch polysaccharide via increasing regulatory T cells. Int J Biol Macromol. 2024;277:134241.
102. Krukowski K, Ma J, Golonzhka O, Laumet GO, Gutti T, van Duzer JH, Mazitschek R, Jarpe MB, Heijnen CJ, Kavelaars A. HDAC6 inhibition effectively reverses chemotherapy-induced peripheral neuropathy. Pain. 2017;158:1126–37.
103. Hu YD, Wang ZD, Yue YF, Li D, Zhen SQ, Ding JQ, Meng W, Zhu HL, Xie M, Liu L. Inhibition of HDAC6 alleviates cancer-induced bone pain by reducing the activation of NLRP3 inflammasome. Int J Mol Med. 2024;53:4.
104. Meltzer S, Santiago C, Sharma N, Ginty DD. The cellular and molecular basis of somatosensory neuron development. Neuron. 2021;109:3736–57.
105. Lallemend F, Ernfors P. Molecular interactions underlying the specification of sensory neurons. Trends Neurosci. 2012;35:373–81.
106. Han W, Lo HW. Landscape of EGFR signaling network in human cancers: biology and therapeutic response in relation to receptor subcellular locations. Cancer Lett. 2012;318:124–34.
107. Wang YN, Hung MC. Nuclear functions and subcellular trafficking mechanisms of the epidermal growth factor receptor family. Cell Biosci. 2012;2:13.
108. Wang YN, Yamaguchi H, Hsu JM, Hung MC. Nuclear trafficking of the epidermal growth factor receptor family membrane proteins. Oncogene. 2010;29:3997–4006.
109. Sorkin A. Cargo recognition during clathrin-mediated endocytosis: a team effort. Curr Opin Cell Biol. 2004;16:392–9.
110. Mayor S, Pagano RE. Pathways of clathrin-independent endocytosis. Nat Rev Mol Cell Biol. 2007;8:603–12.
111. Lo HW, Ali-Seyed M, Wu Y, Bartholomeusz G, Hsu SC, Hung MC. Nuclear-cytoplasmic transport of EGFR involves receptor endocytosis, importin beta1 and CRM1. J Cell Biochem. 2006;98:1570–83.
112. Wang YN, Wang H, Yamaguchi H, Lee HJ, Lee HH, Hung MC. COPI-mediated retrograde trafficking from the Golgi to the ER regulates EGFR nuclear transport. Biochem Biophys Res Commun. 2010;399:498–504.
113. Wang YN, Yamaguchi H, Huo L, Du Y, Lee HJ, Lee HH, Wang H, Hsu JM, Hung MC. The translocon Sec61beta localized in the inner nuclear membrane transports membrane-embedded EGF receptor to the nucleus. J Biol Chem. 2010;285:38720–9.
114 Zajączkowska R, Kocot-Kępska M, Leppert W, Wordliczek J. Bone Pain in Cancer Patients: Mechanisms and Current Treatment. Int J Mol Sci. 2019;20:6047.
115. Zheng XQ, Wu YH, Huang JF, Wu AM. Neurophysiological mechanisms of cancer-induced bone pain. J Adv Res. 2022;35:117–27.
116. Hua B, Gao Y, Kong X, Yang L, Hou W, Bao Y. New insights of nociceptor sensitization in bone cancer pain. Expert Opin Ther Targets. 2015;19:227–43.
117. Hamamoto DT, Khasabov SG, Cain DM, Simone DA. Tumor-evoked sensitization of C nociceptors: a role for endothelin. J Neurophysiol. 2008;100:2300–11.
118. Jing D, Zhao Q, Zhao Y, Lu X, Feng Y, Zhao B, Zhao X. Management of pain in patients with bone metastases. Front Oncol. 2023;13:1156618.
119. Coluzzi F, Mandatori I, Mattia C. Emerging therapies in metastatic bone pain. Expert Opin Emerg Drugs. 2011;16:441–58.
120. Murdaca G, Colombo BM, Puppo F. Anti-TNF-alpha inhibitors: a new therapeutic approach for inflammatory immune-mediated diseases: an update upon efficacy and adverse events. Int J Immunopathol Pharmacol. 2009;22:557–65.
121. Edvinsson L, Ho TW. CGRP receptor antagonism and migraine. Neurotherapeutics. 2010;7:164–75.
122. Bharucha AE, Linden DR. Linaclotide - a secretagogue and antihyperalgesic agent - what next? Neurogastroenterol Motil. 2010;22:227–31.
123. Lu HJ, Wu XB, Wei QQ. Ion channels in cancer-induced bone pain: from molecular mechanisms to clinical applications. Front Mol Neurosci. 2023;16:1239599.
124. Koivisto AP, Voets T, Iadarola MJ, Szallasi A. Targeting TRP channels for pain relief: A review of current evidence from bench to bedside. Curr Opin Pharmacol. 2024;75: 102447.
125. Descalzi G, Ikegami D, Ushijima T, Nestler EJ, Zachariou V, Narita M. Epigenetic mechanisms of chronic pain. Trends Neurosci. 2015;38:237–46.
126. Griffin N, Faulkner S, Jobling P, Hondermarck H. Targeting neurotrophin signaling in cancer: The renaissance. Pharmacol Res. 2018;135:12–7.
127. Damare R, Engle K, Kumar G. Targeting epidermal growth factor receptor and its downstream signaling pathways by natural products: a mechanistic insight. Phytother Res. 2024;38:2406–47.
128. Yin X, Zhao Z, Yin Y, Shen C, Chen X, Cai Z, Wang J, Chen Z, Yin Y, Zhang B. Adverse event profiles of epidermal growth factor receptor-tyrosine kinase inhibitors in cancer patients: a systematic review and meta-analysis. Clin Transl Sci. 2021;14:919–33.
129. Tripathy RK, Pande AH. Molecular and functional insight into anti-EGFR nanobody: Theranostic implications for malignancies. Life Sci. 2024;345:122593.

130. Kersten C, Cameron MG. Cetuximab alleviates neuropathic pain despite tumour progression. BMJ Case Rep. 2012;2012:bcr1220115374.
131. Moryl N, Obbens EA, Ozigbo OH, Kris MG. Analgesic effect of gefitinib in the treatment of non-small cell lung cancer. J Support Oncol. 2006;4:111.
132. Verma V, Khoury S, Parisien M, Cho C, Maixner W, Martin LJ, Diatchenko L. The dichotomous role of epiregulin in pain. Pain. 2020;161:1052–64.

Publisher's Note